Modulation Techniques for Current Ripple Reduction in Five-Phase Induction Motor Drives

Dissertation submitted to
Visvesvaraya National Institute of Technology, Nagpur
in partial fulfilment of the requirements for the award of
the degree

Master of Technology
in
"Power Electronics and Drives"

by

Devendra Ravindra Dhore
(MT23PED004)

Under the Guidance of

Dr. Ramsha Karampuri

Department of Electrical Engineering
Visvesvaraya National Institute of Technology
Nagpur 440010 (India)

June 2025

© Visvesvaraya National Institute of Technology (VNIT) 2009

Department of Electrical Engineering
Visvesvaraya National Institute of Technology

Declaration

I, **Devendra Ravindra Dhore**, hereby declare that this dissertation titled **"Modulation Techniques for Current Ripple Reduction in Five-Phase Induction Motor Drives"** is carried out by me in the Department of Electrical Engineering of Visvesvaraya National Institute of Technology, Nagpur. The work is original and has not been submitted earlier whole or in part of the award of any degree/diploma at this or any other institution/University.

Dhore

Devendra Ravindra Dhore
Date: 30/05/2025

Certificate

This is to certify that the dissertation titled **"Modulation Techniques for Current Ripple Reduction in Five-Phase Induction Motor Drives"** is submitted by **Devendra Ravindra Dhore** in partial fulfillment of the requirements for the award of the degree of **Master of Technology in Power Electronics and Drives,** VNIT Nagpur. The work is comprehensive, complete and fit for final evaluation.

30/05/2025

Dr. Ramsha Karampuri
Assistant Professor,
Department of Electrical Engineering
VNIT, Nagpur

Dr. B.S. Umre
Head, Department of Electrical Engineering
VNIT, Nagpur
Date: 30.05.2025

Department of Electrical Engineering
Visvesvaraya National Institute of Technology

Non-Plagiarism Certificate

Certified that M. Tech Dissertation titled **"Modulation Techniques for Current Ripple Reduction in Five-Phase Induction Motor Drives"** submitted by Devendra Ravindra Dhore, Enrollment No. MT23PED004, ID NO.:30698 has been checked for plagiarism including references using TURNITIN software and the overlap is found within prescribed limits. A summary of report is given below.

ORIGINALITY REPORT

25%	19%	21%	5%
SIMILARITY INDEX	INTERNET SOURCES	PUBLICATIONS	STUDENT PAPERS

Dhore

Devendra Ravindra Dhore
Enrollment No.: MT23PED004
ID No.: 30/698
Date: 30/05/2025

30/05/2025

Dr. Ramsha Karampuri
Assistant Professor,
Department of Electrical Engineering
VNIT, Nagpur

ACKNOWLEDGEMENT

I take this opportunity to express my deepest gratitude to my guide, **Dr. Ramsha Karampuri** for his invaluable guidance, constant encouragement, timely suggestions, and constructive feedback throughout my research work. His support and the excellent research facilities at the **Electrical Drives Lab** significantly contributed to the successful completion of my research.

I am profoundly grateful to **Dr. B.S. Umre**, Head of the Electrical Engineering Department at VNIT, Nagpur.

Thanks, are also due to honourable authorities of Visvesvaraya National Institute of Technology, Nagpur, Lab-Assistant and non-teaching staff of department for their timely help in dealing with office matter and fieldwork.

It would be dishonest of me, if I do not acknowledge the most valuable co-operation in respect of technical supports and valuable suggestion offered by my senior **Mrs. Gunwanti Shende Bharshankar, Miss. Akanksha Karlekar, Mr. Jay Pandit, Mr. L. Charan** and colleague **Harsh Moon**.

Finally, I acknowledge the immense encouragement and support provided by my family, friends, and colleagues. Their support, along with the blessings of the God, has been fundamental to my achievements.

Abstract

The rapid evolution of electric vehicle technology is driven by the necessity to reduce reliance on depleting fossil fuel reserves while ensuring high operational efficiency and sustainability. Multiphase motor drives, particularly five-phase voltage source inverters (VSIs), have gained prominence due to their superior power density and fault tolerance. However, the complexity of controlling these drives requires sophisticated pulse width modulation (PWM) strategies tailored to diverse operating conditions. This study systematically analyses space vector PWM methodologies applicable to five-phase VSIs, specifically Conventional Space Vector PWM (CSVPWM), Bus-Clamped PWM (BCPWM), and Advanced PWM (ADPWM). By leveraging small, medium, and large space vectors, the effectiveness of each technique is evaluated with respect to phase current total harmonic distortion (THD). The findings indicate that BCPWM and ADPWM offer substantial improvements in THD mitigation compared to CSVPWM, particularly at higher modulation index.

Furthermore, this research proposes a hybrid modulation framework integrating conventional and advanced bus-clamping switching sequences for enhanced current ripple suppression in multiphase induction motor drives. The analytical model extends conventional space vector theories by incorporating discontinuous and adaptive modulation strategies, establishing a comparative framework between three-phase and five-phase VSI systems. The study employs the (2L+2M) vector selection methodology to optimize phase current ripple characteristics across various PWM techniques, including CSVPWM, BCPWM, and multiple Advanced Phase Clamped PWM (APCPWM) variants. Simulation and experimental validation confirm that the proposed two-zone hybrid PWM strategy achieves an approximately 23% reduction in phase current harmonic distortion, demonstrating superior performance in maintaining voltage stability and minimizing switching losses at rated operational parameters.

The results underscore the robustness of advanced bus-clamping PWM techniques in improving the dynamic performance of multiphase motor drives, particularly for

applications requiring high power density and stringent harmonic control. The presented approach offers substantial advancements in VSI modulation strategies, establishing a foundation for next-generation electric vehicle propulsion systems and industrial high-performance drive applications. The integration of refined PWM methodologies within five-phase drive architectures enhances inverter efficiency, reduces electromagnetic interference, and supports future scalability in complex multi-motor configurations.

List of Figures

2.1. Phasor Diagram of Five-Phase System……. 8

2.2. Five-Phase Inverter……. 9

2.3. Voltage vectors in $\alpha - \beta$ and $x_3 - y_3$ plane for five-phase VSI…….. 12

2.4. Load Configuration……. 13

2.5. Voltage Vectors Synthesis in (a) $\alpha - \beta$ plane (b) $x_3 - y_3$ plane…….. 14

2.6. Order of Switching Vectors……. 15

2.7. Development of Dwell Times by Projection……. 15

3.1. Partitioning of Zero State for the analyzed space vector PWM technique. The following are as follows: for SVPWM t_{31}= t_0= 0.5t_z; 72^0 Negative Clamp t_{31}= 0, regardless of the sector; 72^0 Positive Clamp t_0= 0……. 20

3.2. Clamp-36^0 (On the Top Left Side-Space Vector Locations, On the Top right side-Gate pulses in the first sector, Bottom is having Sectors, Modulation Index, Gate Pulse of CSVPWM)…….. 21

3.3. 72^0 Positive Clamp (On the Top Left Side-Space Vector Locations, On the Top right side-Gate pulses in the first sector, Bottom is having Sectors, Modulation Index, Gate Pulse of 72^0 positive Clamp)……. 22

3.4. 72^0 Negative Clamp (On the Top Left Side-Space Vector Locations, On the Top right side-Gate pulses in the first sector, Bottom is having Sectors, Modulation Index, Gate Pulse of 72^0 Negative Clamp)……. 23

3.5. Clamp 18^0 (On the Top Left Side-Space Vector Locations, On the Top right side-Gate pulses in the first sector, Bottom is having Sectors, Modulation Index, Gate Pulse of Clamp 18^0)……. 24

3.6. Clamp 36^0 (On the Top Left Side-Space Vector Locations, On the Top right side-Gate pulses in the first sector, Bottom is having Sectors, Modulation Index, Gate Pulse of Clamp 36^0)……. 25

3.7. Clamp 18^0APCPWM 01 (On the Top Left Side-Space Vector Locations, On the Top right side-Gate pulses in the first sector, Bottom is having Sectors, Modulation Index, Gate Pulse of Clamp 18^0 APCPWM 01) ……. 27
3.8. Clamp 18^0APCPWM 02 (On the Top Left Side-Space Vector Locations, On the Top right side-Gate pulses in the first sector, Bottom is having Sectors, Modulation Index, Gate Pulse of Clamp 18^0APCPWM 02) ……... 28
3.9. Clamp 18^0 APCPWM 03 (On the Top Left Side-Space Vector Locations, On the Top right side-Gate pulses in the first sector, Bottom is having Sectors, Modulation Index, Gate Pulse of Clamp 18^0APCPWM 03) ……... 29
3.10. Clamp 36^0APCPWM 01 (On the Top Left Side-Space Vector Locations, On the Top right side-Gate pulses in the first sector, Bottom is having Sectors, Modulation Index, Gate Pulse of Clamp 36^0APCPWM 01) …… … 30
3.11. Clamp 36^0 APCPWM 02 (On the Top Left Side-Space Vector Locations, On the Top right side-Gate pulses in the first sector, Bottom is having Sectors, Modulation Index, Gate Pulse of Clamp 36^0 APCPWM 02) ……. 31
3.12. Clamp 36^0 APCPWM 03 (On the Top Left Side-Space Vector Locations, On the Top right side-Gate pulses in the first sector, Bottom is having Sectors, Modulation Index, Gate Pulse of Clamp 36^0APCPWM 03) …… 32
4.1. Error voltage generation……. 33
4.2. Harmonic flux trajectories for m = 0.75 across a sub-cycle (Ts/2) (a)CSVPWM (b) 72^0 Negative Clamp (c)72^0 Negative Clamp in $\alpha - \beta$ plane (d) above PWM in $x_3 - y_3$ plane……... 36
4.3. Harmonic flux trajectories for m = 0.75 across a sub-cycle (Ts/2) in $\alpha - \beta\ plane$ (a)Clamp 18° (b) Clamp 18° _APCPWM_01(c)Clamp 18° _APCPWM_02 (d) Clamp 18° _APCPWM_03……. 37
4.4. Harmonic flux trajectories for m = 0.75 across a sub-cycle (Ts/2) in $\alpha - \beta\ plane$ (a)Clamp 36° (b) Clamp 36° _APCPWM_01(c)Clamp 36° _APCPWM_02 (d) Clamp 36° _APCPWM_03…… 38
4.5. Harmonic flux trajectories for m = 0.75 across a sub-cycle (Ts/2) (a)both for CSVPWM and BCPWM (b) APCPWM_01(c)APCPWM_02 (d) APCPWM_03…….. 39

4.6. Squared Harmonic flux across $\alpha - \beta$ plane for (a) CSVPWM (b) (b)72^0 Positive Clamp (c)72^0 Negative Clamp (d)Clamp 18^0 (d)36^0Clamp (e) Squared Harmonic flux across $x_3 - y_3$ plane for CSVPWM and BCPWM techniques…… 41
4.7. Squared harmonic flux in $x_3 - y_3$ plane (a) APCPWM_01 (b) APCPWM_02 (c)APCPWM_03…… 42
4.8. Squared harmonic flux at m = 1.0 in $x_3 - y_3$ plane of CSVPWM, BCPWM and advanced PWM Techniques……. 43
4.9. HDF curves show the range of the feasible modulation indices for every PWM technique that was examined . 44
5.1. Flowchart of SVPWM Algorithm…… 48
5.2 The five-phase induction motor and the power and control module are part of the experimental setup 51
5.3. (a) Waveforms for CSVPWM (Top to bottom, Gate Pulse (10ms/div, 2v/div), Phase Voltage (10.0ms/div, 250.0v/div), Phase Current (10ms/div, 5A/div) (b) respective Phase current THD spectrum…… 52
5.4. (a) Waveforms for Clamp 18° (Top to bottom, Gate Pulse (10ms/div, 2v/div), Phase Voltage (10.0ms/div, 250.0v/div), Phase Current (10ms/div, 5A/div) (b) respective Phase current THD spectrum……. 54
5.5. (a) Waveforms for Clamp 36° (Top to bottom, Gate Pulse (10ms/div, 2v/div), Phase Voltage (10.0ms/div, 250.0v/div), Phase Current (10ms/div, 5A/div) (b) respective Phase current THD spectrum…… 54
5.6. (a) Waveforms for Clamp 18°_APCPWM_03 (Top to bottom, Gate Pulse (10ms/div, 2v/div), Phase Voltage (10.0ms/div, 250.0v/div), Phase Current (10ms/div, 5A/div) (b) respective Phase current THD spectrum…… 55
5.7. (a) Waveforms for Clamp 36°_APCPWM_03 (Top to bottom, Gate Pulse (10ms/div, 2v/div), Phase Voltage (10.0ms/div, 250.0v/div), Phase Current (10ms/div, 5A/div) (b) respective Phase current THD spectrum…… 56
5.8. Experimental results Stator current THD versus modulation index for the proposed 36°_$APCPWM$_03 with the conventional CSVPWM, BCPWMs, APCPWM_01 and APCPWM_02……... 57

List of Tables

2.1. Space -Vector of Five-Phase Two-Level Inverter……. 12
3.1. Switching Sequences in Sector 01 for Bus Clamped PWM Techniques..... 19
3.2. Advanced PWM Switching Sequences for Sector 01 Switching Sequence in Sector I…… 26
5.1. Nominal Parameters of FPIM……. 50
5.2. Phase current THD performance evaluation of PWM systems under high modulation Index operation
……. 58

NOMENCLATURE

APCPWM	Advanced Phase Clamped Pulse Width Modulation
BCPWM	Bus Clamped Pulse Width Modulation
CSVPWM	Conventional Space Vector Pulse Width Modulation
NPC	Neutral Point Clamped
PWM	Pulse Width Modulation
SPWM	Sine Pulse Width Modulation
SVPWM	Space Vector Pulse Width Modulation
THD	Total Harmonic Distortion
VSI	Voltage Source Inverter

LIST OF PUBLICATIONS

A. Conference

1. S. A. Sadale, D. R. Dhore and R. Karampuri, **"Current Ripple Analysis of 72° Phase-Clamping PWM Techniques for Five-Phase Drive,"** *2024 IEEE International Conference on Power Electronics, Drives and Energy Systems (PEDES)*, Mangalore, India, 2024, pp. 1-6, doi:10.1109/PEDES61459.2024.10961385.
2. S. A. Sadale, D. R. Dhore and R. Karampuri, **"Improved Phase-Clamping PWM Techniques with Space Vector Approach for Five-Phase System,"** *2024 IEEE International Conference on Power Electronics, Drives and Energy Systems (PEDES)*, Mangalore, India, 2024, pp. 1-6, doi:10.1109/PEDES61459.2024.10961144.

B. Journal

1. Devendra Ravindra Dhore, Sourabh Ashok Sadale and R. Karampuri, **"Advanced Phase-Clamped PWM Techniques for Ripple Current Reduction in Five-Phase Machines,"** IEEE *Transactions on Industrial Electronics (*Submitted for review)

Index

Abstract……. i

List of Figures……... ii

List of Tables……. v

Nomenclature…… vi

List of Publications…… Vii

1. INTRODUCTION……. 1

1.1 Motivation…… 1

1.2 Advantages and Applications of Multi Phase Drives……... 2

1.3 Literature Review……..... 3

1.4 Problem Statement…… 5

1.5 Research Objective…… 6

1.6 Thesis Organization……... 6

2. FIVE-PHASE INVERTER ANALYSIS……. 8

2.1 Introduction……... 8

2.2 Five-Phase Supply System…… 8

2.3 Five-Phase Two-Level VSI…….……. 9

2.4 Modelling of Two-Level SVPWM……... 10

2.4.1 Multiple Space Concept Theory……... 11

2.4.2 Space Vector Timing Calculation……. 13

3. SPACE VECTOR BASED MULTIPHASE MODULATION METHODS. 18

3.1 CSVPWM…… 18

3.2 Bus-Clamped PWM Techniques……. 19

3.3 Advanced Phase-Clamped PWM Techniques……. 26

4. RIPPLE CURRENT ANALYSIS IN MULTIPHASE DRIVE……. 33

4.1 Creation of Ripple in Output Current……. 33

4.1.1 Steps Followed for the Ripple Current Analysis…… 34
4.1.1.1 Harmonic Flux Trajectories……... 34
4.1.1.2 Evaluation of Squared Harmonic Flux……. 39
4.1.1.3 Flux HDF Analysis……..... 43

5. EXPERIMENTAL ANALYSIS AND DSP-BASED IMPLIMENTATION OF PWM TECHNIQUES……..... 46

5.1 Real-time Implementation of PWM Algorithm using DSP TMS320F28379D…… 46
5.1.1 Introduction……. 46
5.1.2 GPIOs (General Purpose Input Output Pins) ……. 46
5.1.3 ePWM (Enhanced Pulse Width Modulator) Module……. 47
5.1.4 ADC (Analog to Digital Converter) and DAC (Digital to Analog Converter) ……. 47
5.1.5 Flowchart Description of PWM Implementation……... 48
5.2 Experimental Analysis……... 49

6. CONCLUSIONS……. 60

Bibliography……... 61

CHAPTER 1
INTRODUCTION

1.1 Motivation

Developing contributions in the area of expanding modulation techniques with applications in multiphase drives is the primary driving force behind this thesis. The creation of a variable-speed drive based on multiphase drives for use in the propulsion of electric vehicles will be the ultimate objective.

Over the past ten years, one of the most influential and rapidly expanding research areas has been the study of electric vehicles. Notwithstanding the advancements in this field, electric vehicles have not yet overtaken conventional vehicles, and support for research in this area is thought to be necessary to strengthen them, especially in areas pertaining to the creation of new and more effective propulsion technologies (electric motors) and energy storage systems (batteries).

An example of these promotional activities in India, for instance, as part of its plan to encourage clean and sustainable transportation, the country has launched a number of programs to hasten the adoption of electric cars (EVs). The National Electric Mobility Mission Plan's (NEMMP) Faster Adoption and Manufacturing of Hybrid and Electric Vehicles (FAME) program is a significant initiative in this regard. FAME-II, the second phase, was introduced in 2019 with a ₹10,000 crore financial investment. It seeks to facilitate the rollout of 7,000 electric buses, 500,000 electric three-wheelers, 55,000 electric four-wheelers, and one million electric two-wheelers. The plan also prioritizes the construction of the required infrastructure, which includes setting up 2,636 charging stations in 62 cities throughout 24 states and union territories.

In addition to central government efforts, several state governments have introduced dedicated EV policies. These policies offer various incentives such as purchase subsidies, tax exemptions, and support for the development of charging infrastructure. India has also set a target of achieving 30% electric vehicle penetration by 2030, aiming to reduce reliance on fossil fuels and improve environmental sustainability.

The propulsion system represents the most important component of an electric vehicle. It has recently attracted the interest of the international scientific community, and this work, which considers the use of multiphase drives, has characteristics that make them suitable for these applications. However, multiphase drive technology is not currently at a mature stage. It is therefore necessary to consolidate the use of multiphase drives in relevant application areas such as the one proposed in this thesis.

1.2 Advantages & Applications of Multi-Phase Drives

Compared to their three-phase predecessors, multi-phase drives have a few clear advantages. Using a multi-phase machine as opposed to a three-phase machine provides the following main benefits:

1. Greater fault tolerance
2. Reduced current per phase for a given voltage rating
3. Lower the power rating of each inverter leg's power electronic components, resulting in simpler and more dependable power conditioning equipment.
4. Reduced copper loss and higher efficiency
5. Reduction in torque pulsation
6. Higher torque density and hence reduced size of the machine for a given power rating
7. Lower DC current ripple
8. Better noise characteristics, higher phase number, increase the frequency of torque pulsation, and hence reduction in torque ripples magnitude.
9. Multi-motor drives using a single inverter.

As previously said, multi-phase drives are very appropriate for certain important domains, such as ship propulsion, more electric airplanes, hybrid electric automobiles, electric traction, and battery-powered applications, despite being inappropriate for general-purpose applications.

There are mainly two reasons for this. The issue of static and dynamic voltage and current sharing arises when power electronics switches are connected in series or parallel in high-power applications. Therefore, in many applications, lower per-phase power is very desirable. Multi-phase drives allow for increased fault tolerance in safety-critical applications.

It has been demonstrated that drive behaviour is not significantly affected by the absence of one or two stages. Additionally, safety is more crucial in this application than price. Multi-phase drives are therefore naturally suited for these uses.

1.3 Literature Review

Previous works on Space-vector PWM, multi-phase, and harmonic elimination strategies have been studied and used as a continuous support of reference throughout this thesis. The significant works that have been studied and should be mentioned are described below in brief.

In this paper [1] "**Pulse width Modulation for Electronic Power Conversion**", Based on mathematical studies and measurable findings from operational controlled drive systems, methods of pulse width modulation for controlling three-phase power converters are presented, along with their specific attributes.

The paper [2] "**An overview of Modern PWM Techniques for Three-Phase Voltage-Controlled Voltage-Source Inverter"** gives a summary of contemporary PWM methods. Modulation-function techniques, voltage space vector techniques, programmed and quasi-programmed techniques, feedback and quasi-feedback techniques, and random techniques are the five categories into which PWM techniques fall.

In the paper [3] "**Relation between Space-Vector Modulation and Three-Phase Carrier-Based PWM: A Comprehensive Analysis,**" the connection between space-vector modulation and carrier-based PWM. Discussions were held regarding the type of carrier, the relationship between the modulating signals and space-vector modulation, and the modulation signals and space vectors.

In the paper [4] "**Triangle-Comparison Approach and Space Vector Approach to Pulse Width Modulation in Inverter-fed Drives,**" the similarity between the two widely used methods—the space-vector technique and the triangle-comparison approach. It highlights the circumstances in which they are comparable and those in which they are not.

In the paper [5] "**Preliminary investigation of an Inverter-fed 5-phase Induction Motor**" details the initial testing of a five-phase induction motor that is fed by

an inverter. The torque pulsation in five phases is one-third that of its three-phase counterpart, as demonstrated in this work.

In the paper [6] "**Multi-phase Induction Machine Drive Research-A Survey**" enumerate the advantages of employing more than three stages for an induction machine, both technically and financially. The numerous special benefits of multi-phase machines are also covered.

The paper [7] "**Multi-phase Induction Motor Drives-A Technology Status Review**" describes in detail the state-of-the-art in multiphase induction drives as of right now. benefits of induction machines with several phases. Multiphase induction machine modelling. Direct torque control and simple vector control. Multiphase voltage source inverters are controlled using PWM.

In the paper [8] "**Modelling and Analysis of Induction Machine Containing Space-harmonics,**" An n-phase winding machine mathematical model that accounts for all MMF harmonics is presented. The Park transformation for the multi-phase machines is thus extended.

In the paper [9] "**Development of Space Vector Modulation Strategies for Five-phase Voltage Source Inverter,**" In order to provide a sinusoidal output voltage devoid of low-order harmonics, a novel space vector modulation technique was introduced that produces voltage in the main domain while canceling out the components in the auxiliary domain.

In the paper [10], "**Multi-phase Space Vector Pulse Width Modulation**" introduced a new nine-phase VSI space vector modulation. Additionally, they found that SVPWM outperforms sin-triangle PWM in terms of DC bus use, voltage THD, and current THD, just like three-phase in multi-phase machines. However, the boost in DC bus utilization brought on by SVPWM decreases as the phase number rises.

In the paper [11] "**Analysis of Multi-phase Space Vector Pulse-Width Modulation Based on Multiple d–q Spaces Concept,**" introduced a new space vector modulation for PMSM applications that is appropriate for non-sinusoidal output voltage. .

In the paper [12], "**Generalised Sinusoidal PWM with Harmonic Injection for Multi-Phase VSIs**" explains the generalized idea of injecting the nth harmonic into n-

phase inverters. This method yields DC bus utilization comparable to SVPWM methods for multi-phase devices.

In the paper [13], **"Unified Voltage Modulation Technique for Real-Time Three-phase Conversion,"** a new voltage modulation method based on the idea of effective time. Because of its intrinsic simplicity, the modulation scheme can be changed in real time with ease.

In the paper [14], **"Advanced Bus-Clamping PWM Techniques Based on Space Vector Approach,"** a comparison of advanced bus-clamping (ABCPWM), bus clamping PWM (BCPWM), and conventional space vector pulse width modulation (CSVPWM). Only one zero state is used in ABCPWM, and an active state is applied twice throughout a subcycle. For a given average switching frequency, ABCPWM approaches decreased harmonic distortion in line currents over both BCPWM and CSVPWM at high modulation indices.

In the paper [15], **"Harmonic Analysis of Advanced Bus-Clamping PWM techniques,"** It introduce Advanced Bus Clamp Pulse Width Modulation (ABCPWM). In ABCPWM sequences, one phase is switched twice, the second phase is switched once, and the third phase is clamped during the subcycle. Compared to traditional space vector PWM and discontinuous PWM, ABCPWM techniques result in less harmonic distortion.

In the paper [16] **"Performance Analysis of Five-Phase System for Various Bus-Clamping Space Vector Based Pulse Width Modulation Methods,"** the space vector-based method for generating the switching sequence for a five-phase system. Using the closest voltage vectors, determine the sector and calculate the duty cycle of the desired reference voltage vector. Using the power factor to switch the energy loss calculation

1.4 Problem Statement

A comprehensive review of the available literature offers a clear conceptual understanding of three-phase and five-phase systems in terms of their drive performance. The PWM techniques discussed in the literature present extensive methods for enhancing system performance.

Among these, space vector approach-based PWM techniques stand out as a more general and effective method compared to other PWM techniques. The aim of this study,

in contrast to other research papers, is to generate various PWM techniques by using a zero-space vector, medium space vector, and large space vector, to have bus-clamped PWM techniques in a five-phase system by a space vector-based approach

. Along with the bus-clamped PWM techniques, design some other PWM techniques to have better performance in terms of harmonic contents and their total harmonic distortion.

1.5 Research Objective

The objective of this thesis is to study multiphase drives, focusing on five induction machines, their analysis, and the extension of modulation strategies used in conventional three-phase drives. Specifically, the following objectives can be listed:

1. To extend continuous and discontinuous PWM modulation algorithms to multiphase drives, establishing a unique relationship between carrier-based and SV-based modulation strategies.

2. To establish a methodology for the comparative analysis of modulation strategies that can be used in multiphase two-level input power converters for multiphase machines, in order to subsequently identify the comparative advantages and disadvantages of these modulation strategies in the multiphase case, as well as their respective scope of use.

1.6 Thesis Organization

Chapter 1 comprises the reasons behind multi-phase drives. The literature review pertaining to various SVPWM algorithms is described, along with problem statements and research goals, and the intrinsic benefits and uses of multi-phase drives are discussed.

Chapter 2 concise explanations of the five-phase VSI's ten-step operating mechanism. Additionally reviewed is the carrier-based sinusoidal PWM for five-phase applications. especially the application of a space vector-based PWM method in a voltage source inverter with five phases.

Chapter 3 presents the proposed SVPWM algorithms for the two-level five-phase system for discontinuous and advanced PWM methodologies.

Chapter 4 describes in detail about switching ripple characteristics of proposed PWM techniques using the space vector approach by harmonic flux evaluation.

Chapter 5 Analyses about hardware results obtained and provides a comparison of different implementation methods. A brief overview of the DSP TMS320F28379D is covered, along with its use in the implementation of the proposed PWM techniques

Chapter 6 summarizes the conclusion of the research findings, along with the future scope

MATLAB has been utilized in this thesis for result visualization, modelling, and general analysis. Code Composer Studio (CCS) was used to create DSP programs. Microsoft Office has also been used to prepare theses.

CHAPTER 2

FIVE-PHASE INVERTER ANALYSIS

2.1 Introduction

The five-phase system and the five-phase inverter are analysed in this chapter. Five-phase systems have different line voltages. The adjacent and non-adjacent line voltages are the two types of line voltages. Analysis is done on the relationships between the line and phase voltages, and five-phase SPWM is explained.

2.2 Five-Phase Supply System

The phasor diagram of a balanced five-phase system is shown in Fig. 1. V_A is taken as the reference voltage, and the phase sequence is A, B, C, D, and E. If the voltages are balanced and equal (i.e.) $Vph = V_A = V_B = V_C = V_D = V_E$ then there is a phase shift of 72º between each phase.

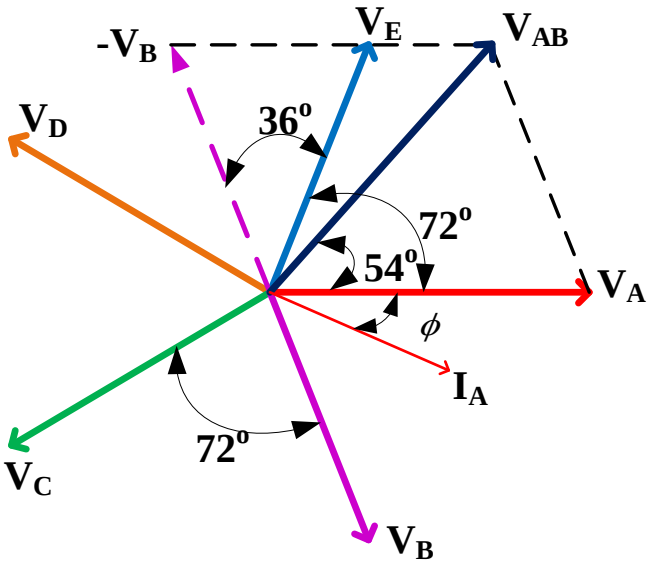

Fig. 2.1 Phasor Diagram of Five-Phase System

The adjacent line voltage is given by

$$V_{AB} = V_A - V_B = V_{ph}\angle 0° - V_{ph}\angle -72° = 1.17557\, V_{ph}\angle 54° \qquad (2.1)$$

The non-adjacent voltage is given by

$$V_{AC} = V_A - V_c = V_{ph}\angle 0° - V_{ph}\angle -144 = 1.9021\, V_{ph}\angle 18° \qquad (2.2)$$

The power in a five-phase system is given by

$$P = 5\,V_{ph}I_{ph}\cos(\phi)\ \ or\ P = 4.25\,V_L I_L \cos(\phi) \qquad (2.3)$$

Therefore, the five-phase power is 2.52 times more than the three-phase power and five times the single-phase power.

2.3. FIVE-PHASE TWO-LEVEL VSI

The front-side converter structure of a five-phase inverter is comparable to that of a three-phase inverter. For the sake of simplicity, the input in the power circuit topology of a five-phase voltage source inverter is taken to be a DC source in Fig. 2.2. It features five legs, with one upper and one lower switch on each leg that complements the others. S1', S2', S3', S4', and S5' are the names of the lower switches, while S1, S2, S3, S4, and S5 are the names of the upper switches.

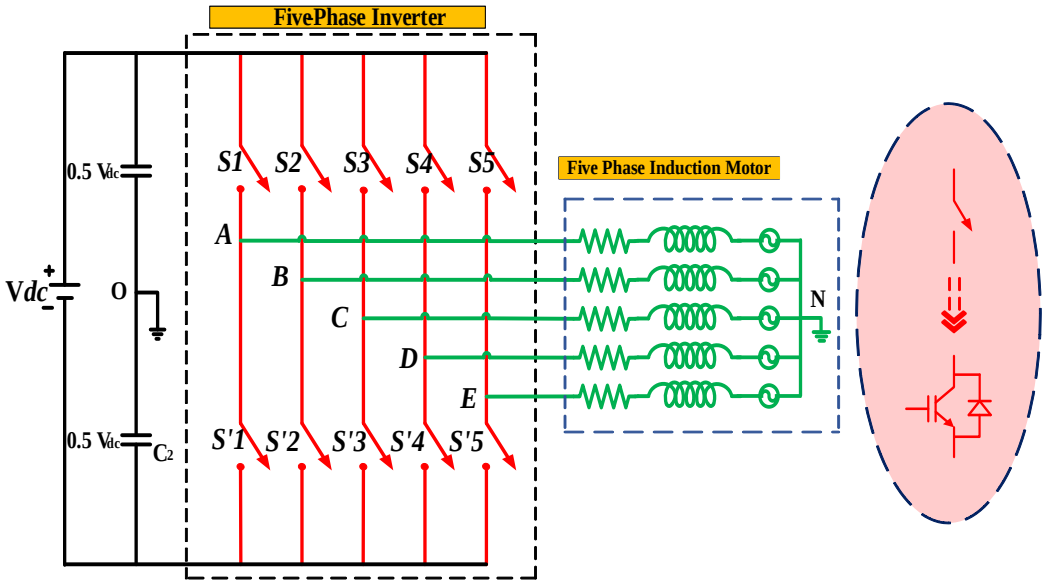

.

Fig. 2.2 Five-Phase Inverter

The voltage between the output phase and DC neutral point O is termed as leg voltage or pole voltage. The voltage between the output phase and the AC neutral point N is termed the phase voltage.

The line voltage in a five-phase case is of two types, one is termed as adjacent line voltage and the other is termed as non-adjacent line voltage. The voltage between two

adjacent-phase for example, between phase A and B, throughout this thesis adjacent line voltage is specified as line voltage only.

The non-adjacent line voltage is the voltage between the two non-adjacent phases, for example, the voltage between phase A and phase C.

2.4. MODELING OF TWO-LEVEL SVPWM

In a two-level five-phase inverter as shown in Fig. 2.2 each phase output of the inverter can attain either $+0.5V_{dc}$ or $-0.5V_{dc}$ with respect to DC midpoint O (if the DC bus has midpoint) (or) V_{dc} or 0 with respect to DC negative bus N (if the DC bus does not have midpoint), i.e., only two states are possible. Hence, the total number of stationary vectors possible is $2^5 = 32$.

2.4.1. Multiple Space Concept Theory

With the exception of the 6n±1)th harmonics corresponding to zero-sequence components, all of the sixn±1)th harmonics of three-phase variables in a three-phase system can be represented equivalently by the following two-dimensional (2-D) complex vector, or space vector on a stationary reference frame.

Three-phase variables' fundamental harmonic can be thought of as a DC component by using the space vector. This concept is essential to a three-phase motor's synchronous frame current control and field-oriented vector control. It is also possible to apply this space vector concept to a five-phase motor. The analogous transformation of five-phase variables should be defined using two space vectors since, except for zero-sequence components, five-phase variables have four degrees of freedom. These two space vectors can be reasoned out because five-phase motor has the following two kinds of phase displacements according to the harmonics of winding density distribution.

1. The A, B, C, D, and E phases are displaced counterclockwise by the (10n±1)th harmonics of the winding density distribution.
2. In the winding density distribution, the A, C, E, B, and D phases are displaced counterclockwise by the (10n±3)th harmonics.

By extending the Clarke transformation for a five-phase system, (2.1) can be used to define the transformation matrix for converting a five-phase system to a two-phase system with the output phases connected in star with the single neutral point.

$$C_5 = \frac{2}{5}\begin{bmatrix} 1 & cos\phi & cos2\phi & cos3\phi & cos4\phi \\ 0 & sin\phi & sin2\phi & sin3\phi & sin4\phi \\ 1 & cos2\phi & cos4\phi & cos6\phi & cos8\phi \\ 0 & sin2\phi & sin4\phi & sin6\phi & sin8\phi \\ \frac{1}{2} & \frac{1}{2} & \frac{1}{2} & \frac{1}{2} & \frac{1}{2} \end{bmatrix} \quad (2.4)$$

Where $\phi = 2\pi/5$, The five-phase symmetrical physical quantities in the natural coordinate system can be projected to two orthogonal planes using this transformation matrix. $\alpha - \beta$ and $x_3 - y_3$.The two orthogonal planes' voltage space vector can be described as follows.

$$\begin{aligned} V_{\alpha\beta} &= V_\alpha + jV_\beta \\ &= \frac{2}{5}\left(V_a + V_b e^{j\phi} + V_c e^{j2\phi} + V_d e^{j3\phi} + V_e e^{j4\phi}\right) \end{aligned} \quad (2.5)$$

$$\begin{aligned} V_{x_3y_3} &= V_{x_3} + jV_{y_3} \\ &= \frac{2}{5}\left(V_a + V_b e^{j2\phi} + V_c e^{j4\phi} + V_d e^{j6\phi} + V_e e^{j8\phi}\right) \end{aligned} \quad (2.6)$$

Table 2.1 displays the stationary vectors that were produced using equations (2.4) and (2.5). These vectors can be broadly categorized as zero vectors or states and active switching vectors or states, which occur when power moves from the input/DC link side of the inverter to the output/load side of the inverter.

Based on their magnitude values, the active vectors for five-phase inverters are further divided into three categories: Large Vectors ($\bar{V}_{al}$) Medium Vectors ($\bar{V}_{bl}$), and Small Vectors. ($\bar{V}_{cl}$)

According to the switching patterns, a five-phase inverter can have two load equivalent circuits: one with one impedance in series with a group of four parallel impedances, and another with two impedances in parallel with a series combination of three parallel impedances, as seen in Fig. 2.4.

Fig 2.3 displays the main plane's and auxiliary plane's space vectors. A decagon is created by joining the tips of the space vectors. Ten separate sectors make up the decagon, which spans more than 360°.

Table 2.1 Space Vectors of Five-Phase Two-Level Inverter

Space Vector	Space vector value	Number of vectors
Large Vectors ($\bar{v}_l$)	$\left(\frac{2}{5}\right)2V_{dc}\cos\left(\frac{\pi}{5}\right)\exp\left(\frac{jm\pi}{5}\right)$ $m = 0,1,...9$	10
Medium Vectors ($\bar{v}_m$)	$\left(\frac{2}{5}\right)V_{dc}\exp\left(\frac{jm\pi}{5}\right)$ $m = 0,1,...9$	10
Small Vectors ($\bar{v}_s$)	$\left(\frac{2}{5}\right)2V_{dc}\cos\left(\frac{2\pi}{5}\right)\exp\left(\frac{jm\pi}{5}\right)$ $m = 0,1,...9$	10
Zero Vectors ($\bar{v}_0, \bar{v}_{31}$)	0	2

While the reference vector $\bar{V}^*$ rotates at the speed of the inverter output voltage's fundamental frequency, the space vectors remain motionless. It goes around once for a single fundamental cycle frequency.

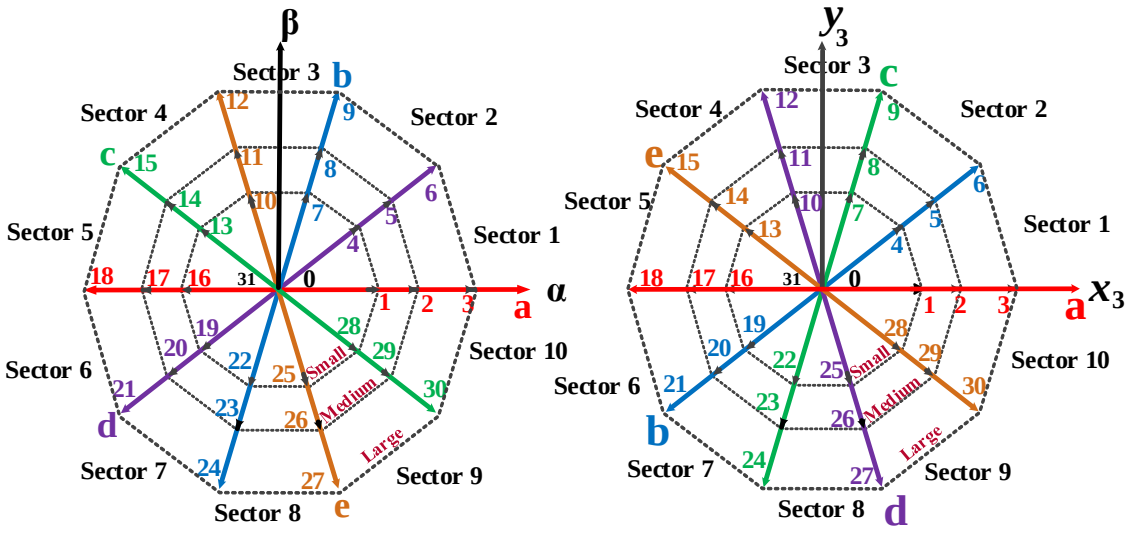

Fig. 2.3 voltage vectors in $\alpha - \beta$ and $x_3 - y_3$ plane for five-phase VSI

Although the zero state vectors are redundant, their purpose is to reduce the frequency of switching.

The frequency and amplitude of the inverter's output voltages are identical to the reference voltage's speed and magnitude)..

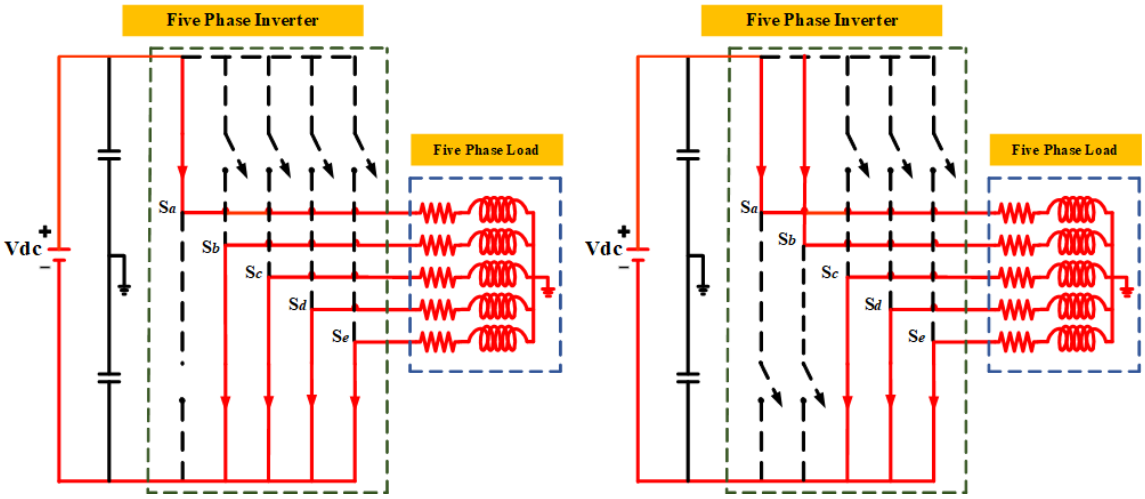

Fig. 2.4 Load configuration

2.4.2 Space Vector Timing Calculation

The component in $x_3 - y_3$ planes suggest another possible sequence of five-phase voltages. This sequence component is if non-zero, produces an output voltage waveform which is non-sinusoidal and which is rich in third harmonics. Hence, the vector domain of the five-phase systems is twofold, with one space producing the second or auxiliary domain, which generates third harmonic voltages embedded in the fundamental voltage, and the fundamental component of voltage, if not specially cancelled. Hence, a simple extension of the two-nearest vector method for three-phase is not suitable for five-phase applications, which need a sinusoidal output voltage.

On the other hand, the nearest two vector method yields the highest DC bus utilization and high-power density in the case of non-sinusoidal machines. Hence the choice of generation of sinusoidal and non-sinusoidal greatly depend on the type of winding of machine, if the windings are sinusoidally distributed then output voltage should be free of all order harmonics like 3^{rd}, 5^{th} etc and It is advisable to inject a specific quantity of voltage harmonics if the windings are focused because this will increase the creation of torque. As mentioned earlier, this project concentrates only on the development of the SVPWM algorithm, which generates sinusoidal voltage free from low-order harmonics. Thus, there exists more than one method of implementing SVPWM in a multi-phase voltage source inverter. However, a five-phase inverter's optimal SVPWM should meet a number of specifications.

1. Each switch can only change states twice during the switching period (once from "ON" to "OFF" and once from "OFF" to "ON," and vice versa) in order to maintain a constant switching frequency and minimize switching loss.
2. The plan needs to optimizes the use of available DC bus
3. The inverter's low-order harmonics should be reduced.

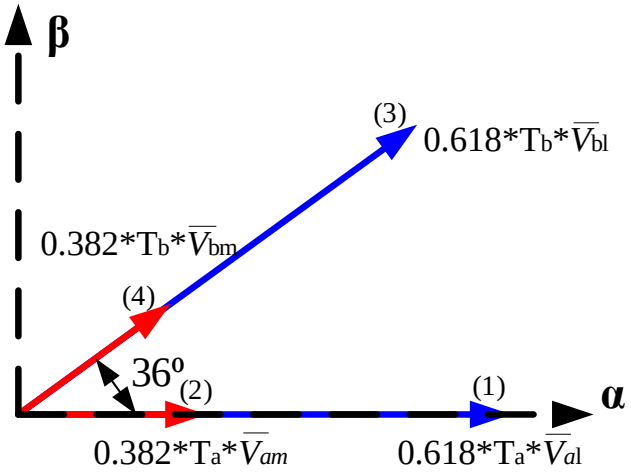

(a)

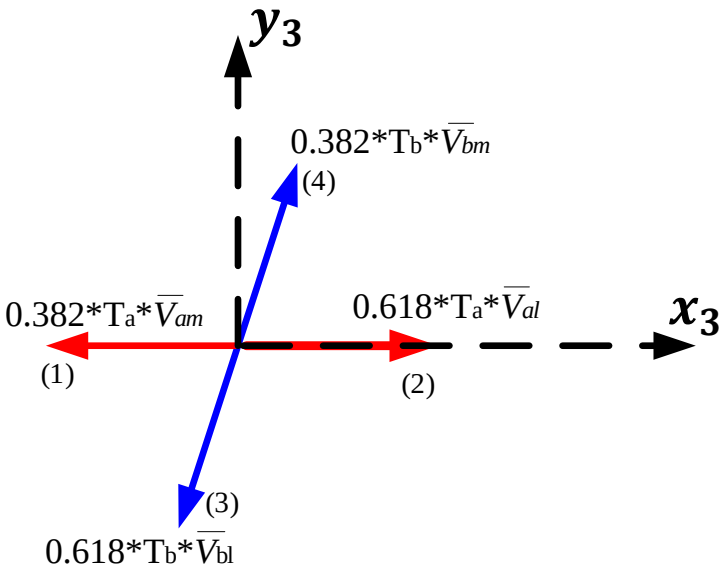

(b)

Fig. 2.5 Voltage Vectors Synthesis in (a) $\alpha - \beta$ plane (b) $x_3 - y_3$ plane

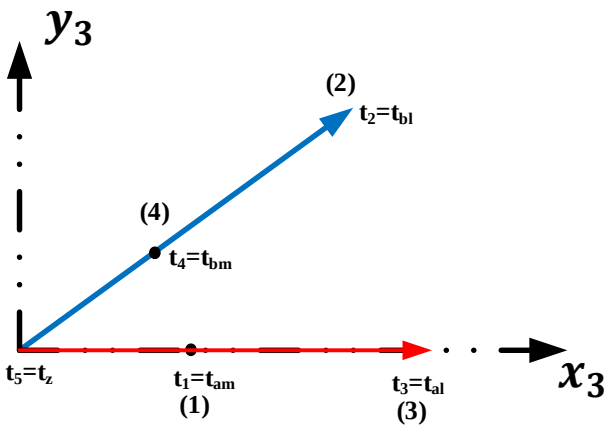

Fig. 2.6 Order of Switching Vectors

These standards are applied while evaluating the advantages and disadvantages of different SVPWMs. Based on the above-mentioned conditions, it was proved in the paper [10] that in a case of- phase inverter, one has to apply four nearest four vectors in order to produce a sinusoidal voltage as explained in detail below. Generally speaking, in order to produce a sinusoidal output voltage for n-phase VSI, n-1 active vectors must be applied during each sampling interval.

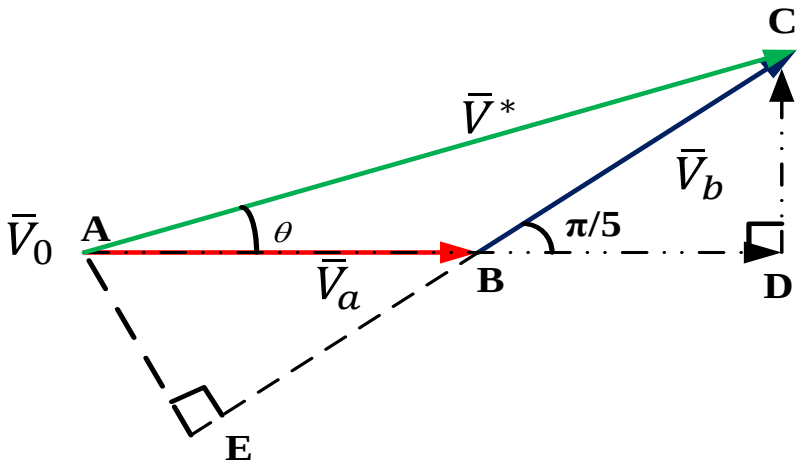

.

Fig. 2.7 Development of Dwell Times by Projection

In order for a five-phase inverter to produce a sinusoidal voltage devoid of third harmonics, the average voltage in the auxiliary frame $\alpha - \beta$ should be zero for every sampling interval. This can be accomplished by giving the larger vector's switching duty 1.618 times the weight of the medium vector. The ratio of the large and medium vectors' magnitudes alone is used to calculate the factor 1.618.

The condition is graphically explained in Fig. 2.5(a) and Fig. 2.5(b), which shows that if we apply as per above said condition (i.e., large vector ($\bar{V}_{al}$ & $\bar{V}_{bl}$)duty cycle is 1.618 times more than medium vector $\bar{V}_{am}$ & $\bar{V}_{bm}$ then the average voltage in the $\alpha - \beta$ plane in a sampling interval is zero with reference to Fig. 2.6 and Fig. 2.7. The voltage components V_a and V_b to be formulated by PWM can be written as follows.

$$V_b \sin\left(\frac{\pi}{5}\right) = \bar{V}^* \sin(\theta) = V_b = \frac{\bar{V}^* sin(\theta)}{\sin\left(\frac{\pi}{5}\right)} \tag{2.7}$$

$$V_a \sin\left(\frac{\pi}{5}\right) = \bar{V}^* \sin\left(\frac{\pi}{5} - \theta\right) = V_b = \frac{\bar{V}^* sin\left(\frac{\pi}{5} - \theta\right)}{\sin\left(\frac{\pi}{5}\right)} \tag{2.8}$$

If the dwell time of the two components V_A and V_A of the voltage $\bar{V}^*$, is formulated by the dwell time of the state as per Fig. 3.4 by weighting the state of the longer vector to be larger than the medium vector by k=1.618 times , to make the auxiliary vectors cancel, then for all vectors dwell times are given as per the following equations.

$$\mathrm{t_{am}} = \frac{2\bar{V}^* sin\left(\frac{\pi}{5} - \theta\right)}{5V_{dc} \sin\left(\frac{\pi}{5}\right)} * \frac{1}{1+k^2} \tag{2.9}$$

$$\mathrm{t_{al}} = \frac{2\bar{V}^* sin\left(\frac{\pi}{5} - \theta\right)}{5V_{dc} \sin\left(\frac{\pi}{5}\right)} * \frac{k}{1+k^2} \tag{2.10}$$

$$\mathrm{t_{bm}} = \frac{2\bar{V}^* sin(\theta)}{5V_{dc} \sin\left(\frac{\pi}{5}\right)} * \frac{1}{1+k^2} \tag{2.11}$$

$$\mathrm{t_{bl}} = \frac{2\bar{V}^* sin(\theta)}{5V_{dc} \sin\left(\frac{\pi}{5}\right)} * \frac{k}{1+k^2} \tag{2.12}$$

were

k = weighting factor of the large vector compared to the medium vector.

$\bar{V}^*$ =Reference vector

θ = Angle of reference vector

V_{dc} = DC bus voltage

For the multi-phase inverter, the maximum DC bus consumption in the linear modulation range for generating the sinusoidal output voltage is provided by

$$\text{DC bus utilization} = \frac{V_{AO(\max)}}{V_{dc}} = \frac{1}{\cos\left(\frac{\pi}{2n}\right)} = 1.05146 \qquad (2.13)$$

Where n = number of phases

Hence, in case of SVPWM based on the nearest four vector method for five-phase applications, the DC bus utilization if 5.1456% more than the SPWM.

CHAPTER 3

SPACE VECTOR BASED MULTIPHASE MODULATION METHODS

For a variety of phase values, sinusoidal output voltages can be produced using the space vector PWM and continuous carrier-based PWM approaches that have been developed for VSI control. Discontinuous PWM techniques are used in PWM systems for five- and seven-phase inverters. The equivalent continuous and discontinuous PWM approaches have been investigated more thoroughly than advanced multiphase PWM techniques. Different PWM approaches yield different results in terms of the performance measures that may be used to assess the output waveforms.

3.1 CSVPWM

Assuming that the machine has a star-connected winding with an isolated neutral point, the Clarke decomposition theory states that the five-phase VSI is characterized by 32 space vectors (30 active + two zero states), with projections in two orthogonal planes, as illustrated in Fig. 2.3 – Fig. 2.3(b). Four active vectors must be chosen in order to zero the voltage (on average) in the second $(x_3 - y_3)$ plane and obtain the desired reference in the first $(\alpha - \beta)$ plane.

Among the two SVPWM approaches that are now available [25], the active vectors are either chosen as two medium and two large vectors that border the reference in the first plane (referred to as the (2L+2M) method) or as four large vectors that border the reference (referred to as the (4L) method). The DC bus voltage is used in the same way as the (2L+2M) and (4L) CSVPWM approaches, regardless of the vector selection mechanism [25].

Additionally, the two zero states have the same and equal temporal length of the zero vectors (T_z). In contrast to the (4L) approach, the current study solely takes into account (2L+ 2M) since it offers total control over the linear modulation range and least harmonic content [32]. The temporal length of specific active vectors is given by equations (2.9) through (2.12), which are generally applicable to all sectors. The applied vector sequence for odd and even sectors differ significantly and is provided as

1. Odd Sector: 0, 2, 6, 3, 5, 31, 31, 5, 3, 6, 0
2. Even Sector: 31, 5, 3, 6, 2, 0, 0, 2, 6, 3, 5, 31

3.2 Bus-Clamped PWM Techniques

One zero voltage vector during a switching phase can be used to convert the (2L+2M) continuous SVPWM techniques to discontinuous approaches. Despite the fact that an endless number of discontinuous patterns can be created, the four pertinent examples are referred to as

1. 72° Positive Clamp
2. 72° Negative Clamp
3. Clamp 18°
4. Clamp 36°

One VSI leg's switching state remains constant during the switching period, which is the primary effect of employing a discontinuous approach. The many zero state partitioning strategies that provide continuous and all of the discontinuous modulation techniques covered in this work are displayed in Table 3.1. Followed by the figures providing space vector locations and gate pulses in the first sector, along with the nature of gating pulses for the whole cycle of the respective PWM techniques as outlined in Fig 3.1 – Fig. 3.6, respectively.

The modulation method Clamp 36° and Clamp 18° is derived from 72° Positive Clamp and 72° Negative Clamp dependent on the sector. For example, Clamp 36° is like 72° Negative Clamp in sector 1, but like72° Positive Clamp in sector 2; Clamp 18° is the same as 72° Positive Clamp While it is similar in the first half of Sector 1 and the second half of Sector 2, 72° Negative Clamp in between sectors.1 and sector 2.

TABLE 3.1

Switching Sequences in Sector 01 for Bus Clamped PWM Techniques

Sr. No.	PWM Techniques	Switching Sequence in Sector 01	Sector Angle
1	72° Positive Clamp	31,5,3,6,2,2,6,3,5,31	36°
2	72° Negative Clamp	0,2,6,3,5,5,3,6,2,0	36°
3	Clamp 18	0,2,6,3,5,5,3,6,2,0	18°
4	Clamp 36°	31,5,3,6,2,2,6,3,5,31	18°

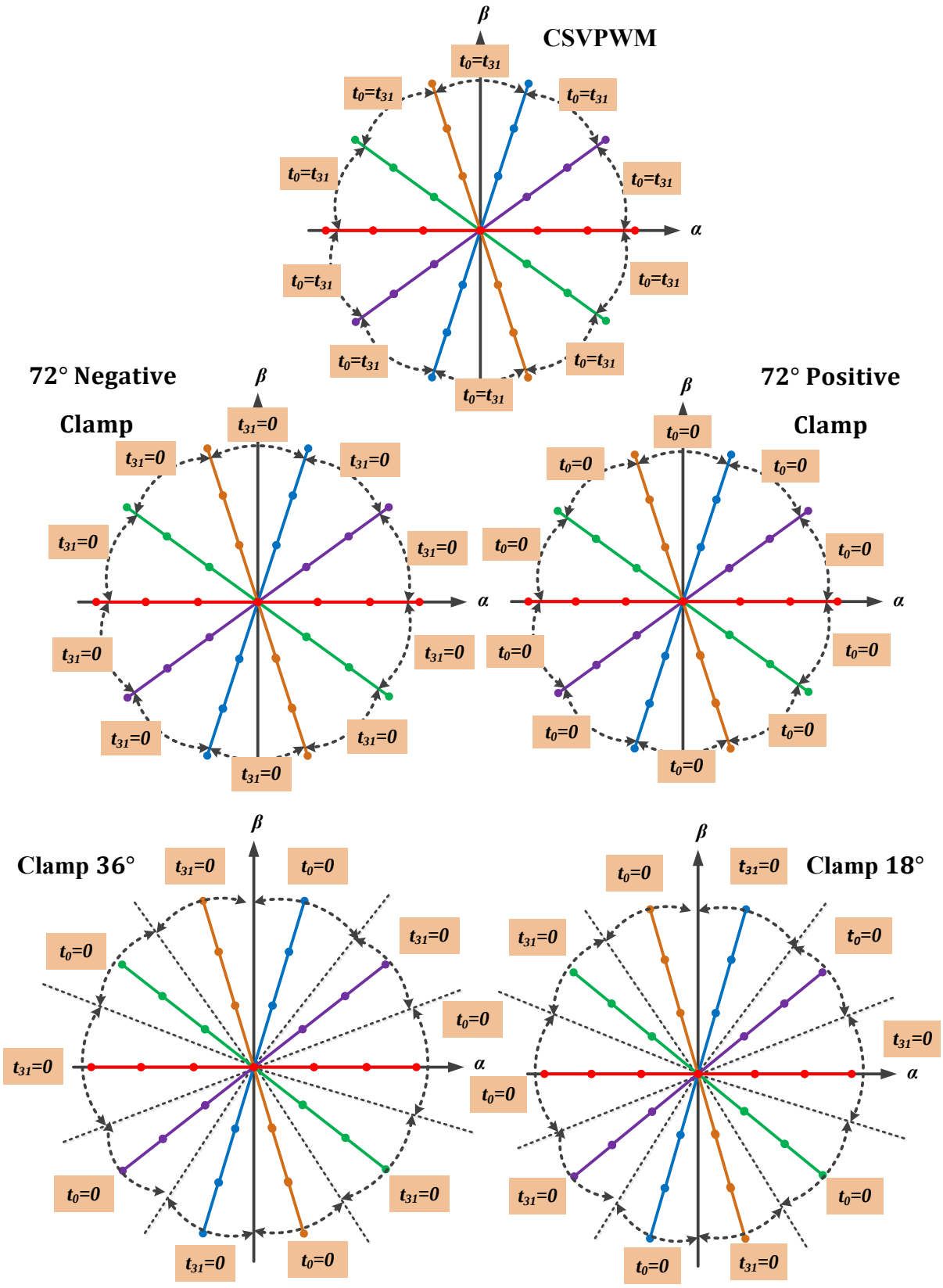

Figure 3.1. Partitioning of Zero State for the analyzed space vector PWM technique. The following are as follows: for SVPWM $t_{31} = t_0 = 0.5t_z$; 72^0 Negative Clamp $t_{31} = 0$, regardless of the sector; 72^0 Positive Clamp $t_0 = 0$.

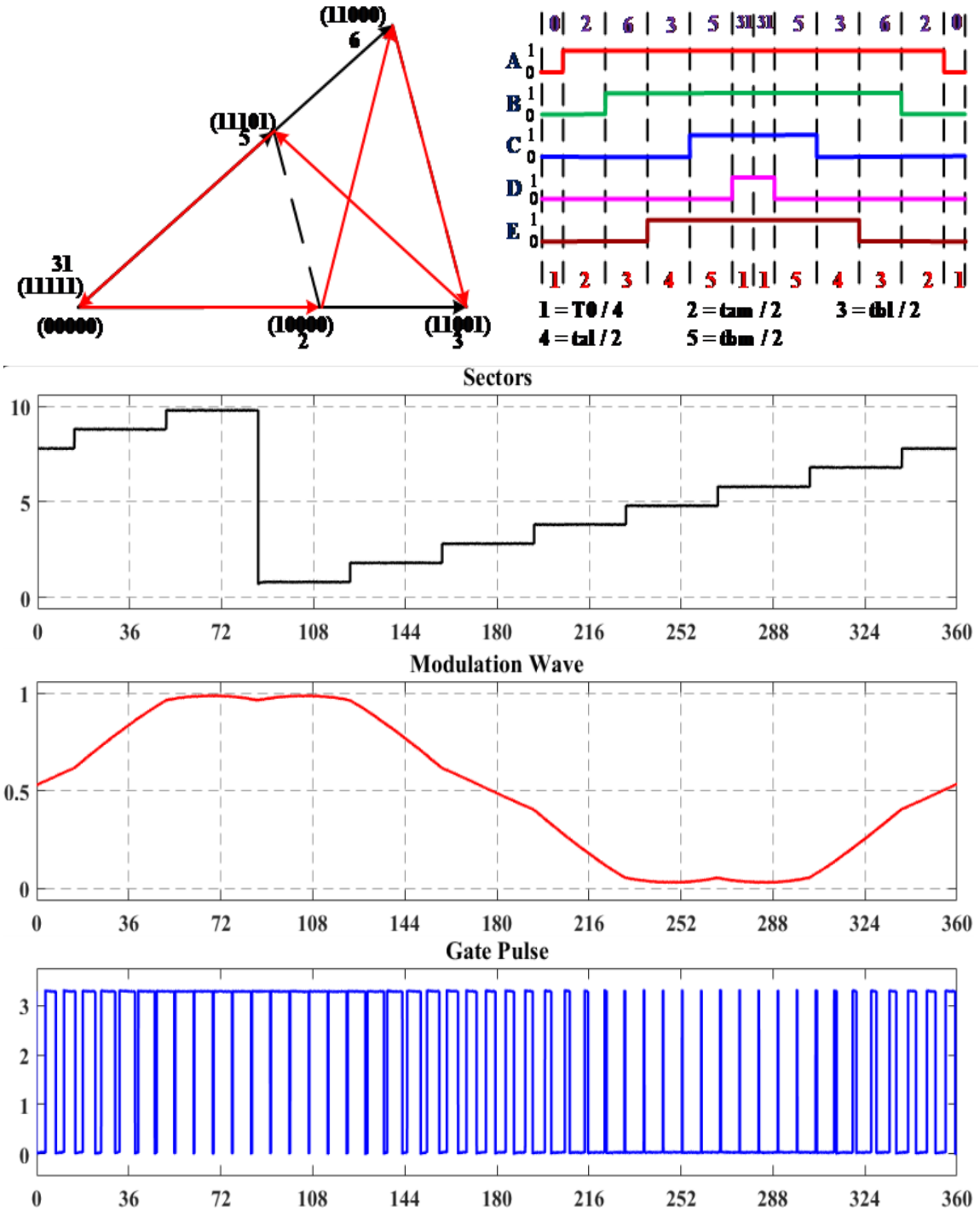

Figure 3.2. Clamp-36^0 (On the Top Left Side-Space Vector Locations, On the Top right side-Gate pulses in the first sector, Bottom is having Sectors, Modulation Index, Gate Pulse of CSVPWM)

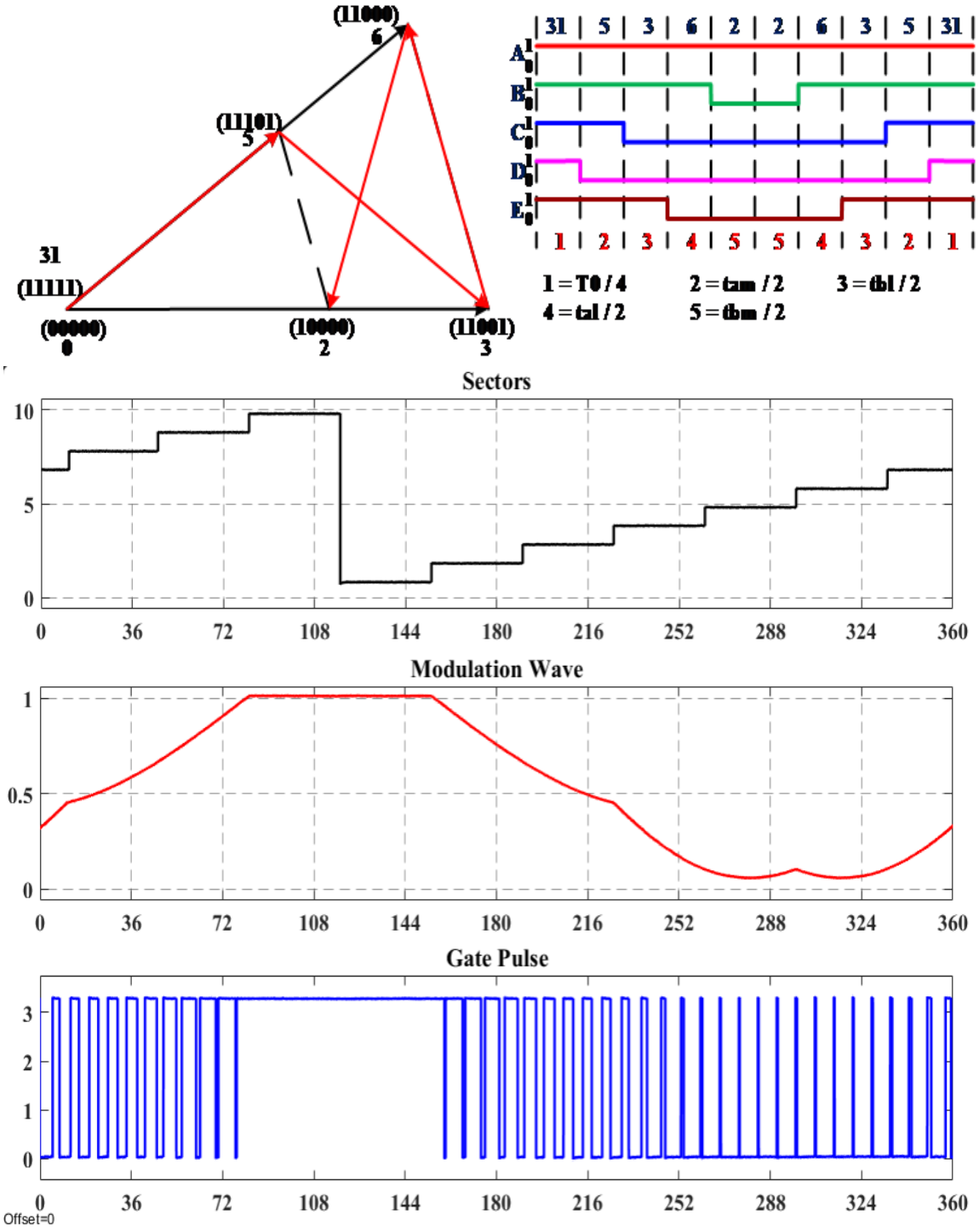

Figure 3.3. 72^0 Positive Clamp (On the Top Left Side-Space Vector Locations, On the Top right side-Gate pulses in the first sector, Bottom is having Sectors, Modulation Index, Gate Pulse of 72^0 positive Clamp)

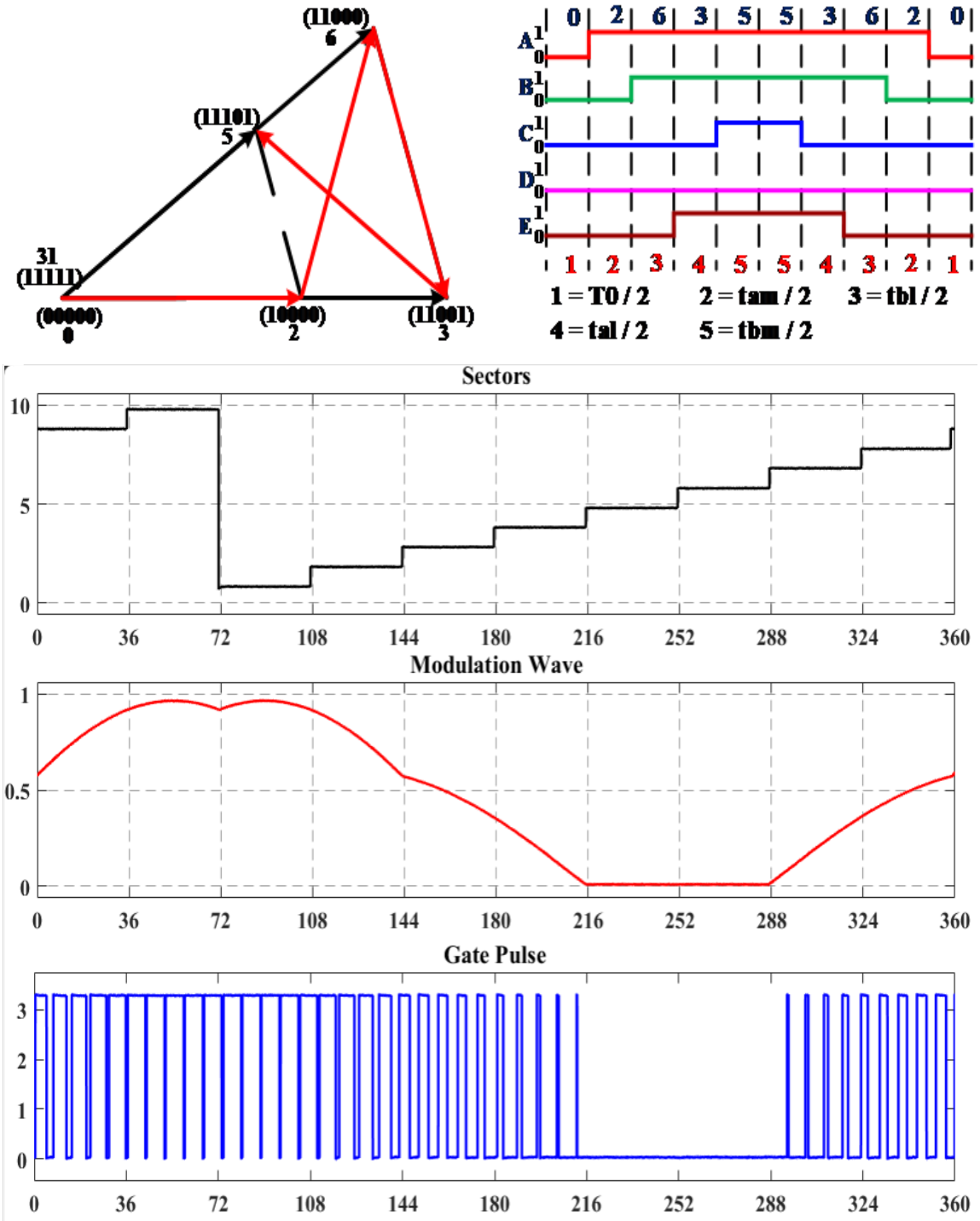

Figure 3.4. 72^0 Negative Clamp (On the Top Left Side-Space Vector Locations, On the Top right side-Gate pulses in the first sector, Bottom is having Sectors, Modulation Index, Gate Pulse of 72^0 Negative Clamp)

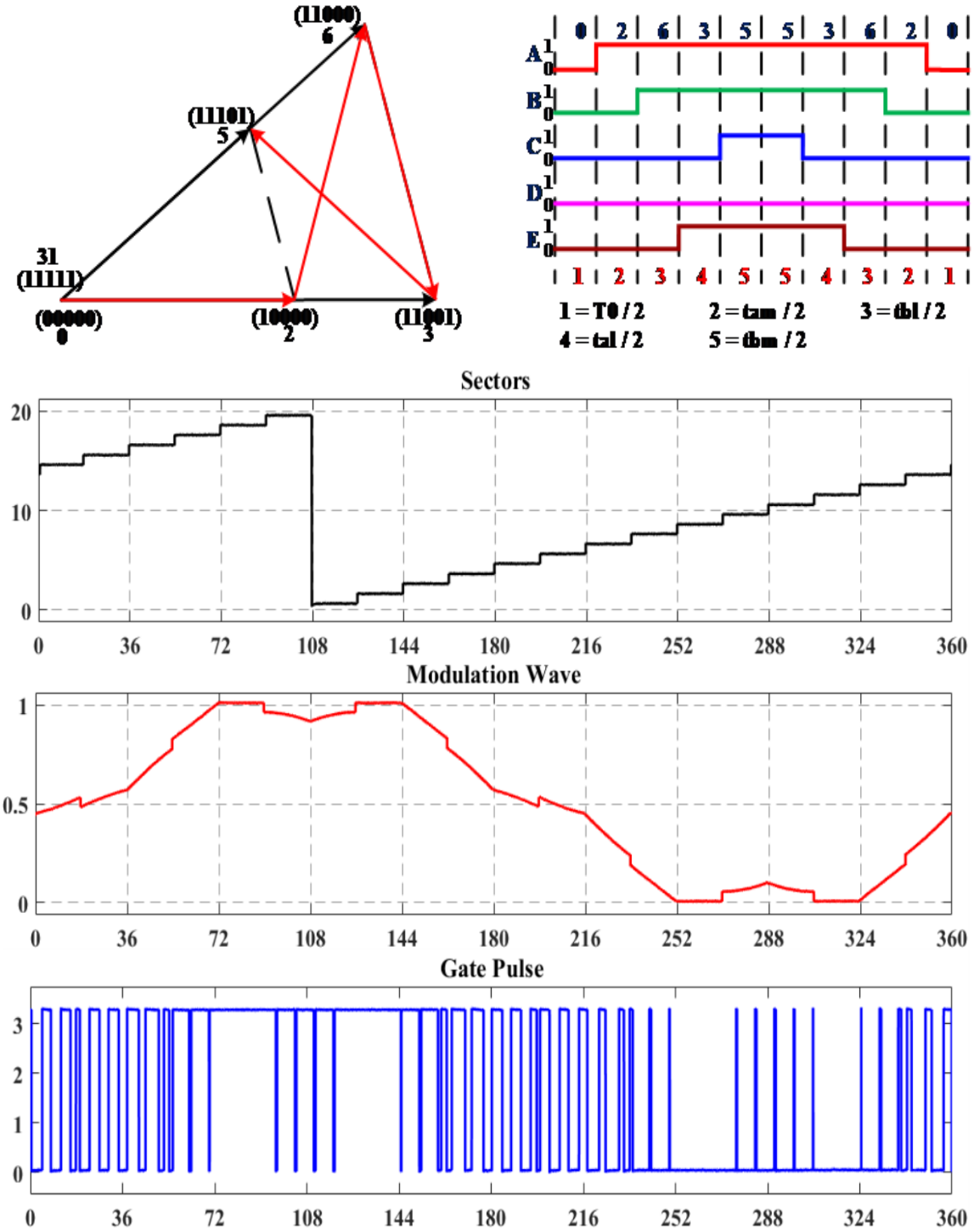

Figure 3.5. Clamp 18^0 (On the Top Left Side-Space Vector Locations, On the Top right side-Gate pulses in the first sector, Bottom is having Sectors, Modulation Index, Gate Pulse of Clamp 18^0)

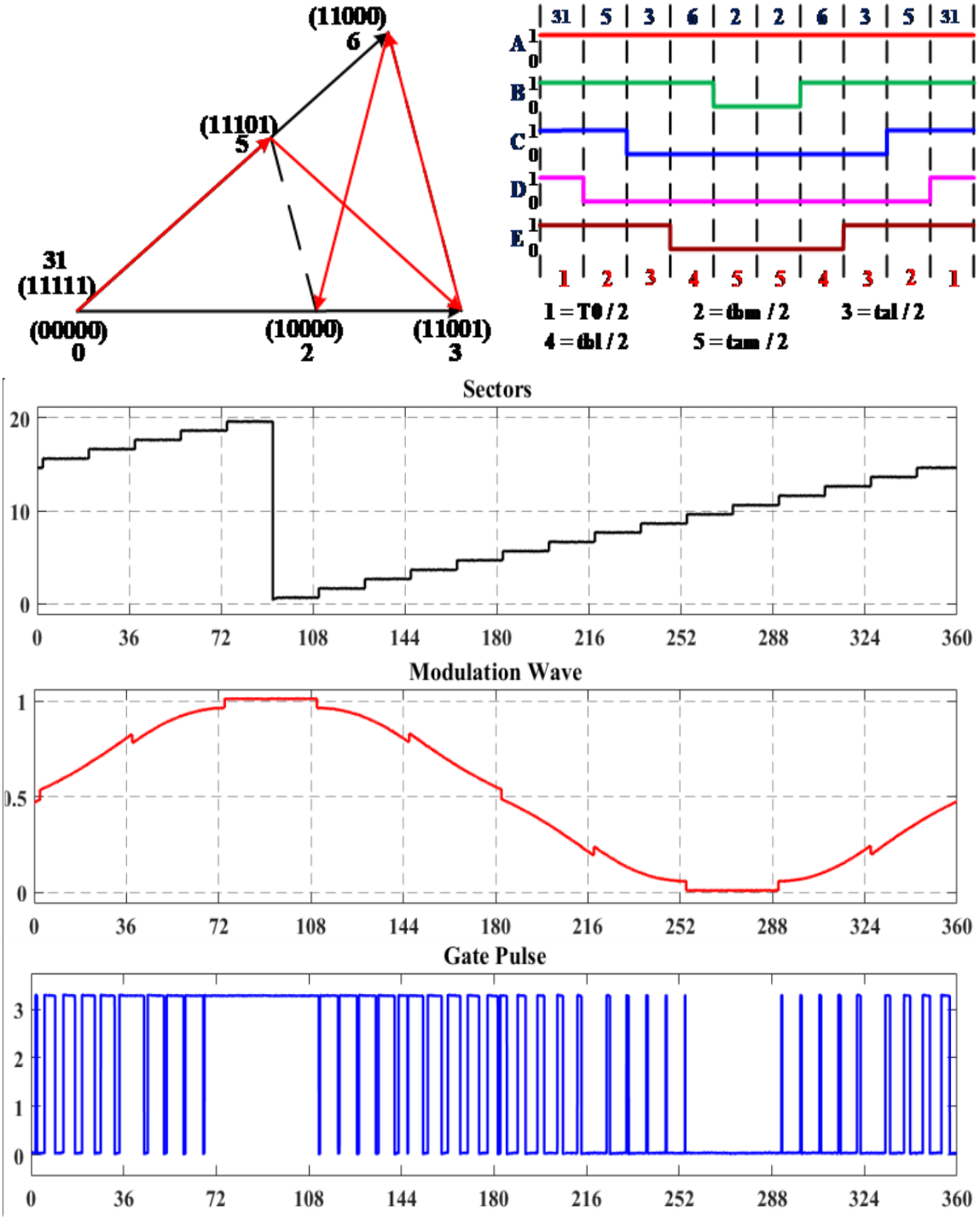

Figure 3.6. Clamp 36^0 (On the Top Left Side-Space Vector Locations, On the Top right side-Gate pulses in the first sector, Bottom is having Sectors, Modulation Index, Gate Pulse of Clamp 36^0)

3.3 Advanced Phase-Clamped PWM Techniques

The different choices for the division of the active vectors' duty cycle subdivision led to the Advanced bus clamped PWM techniques. This article brings out class of open-loop advanced BCPWM techniques, which are an extension of the cases known for three-phase advanced bus-clamping PWM techniques [18]-[29]. The line current distortion due to the proposed PWM techniques is studied and compared against those due to CSVPWM and BCPWM. The conventional sequence in a five-phase system consists of two zero and four active vectors, which gives more degrees of freedom, as in the case of a three-phase system for designing the sequences of advanced PWM techniques. Since an active vector can be applied more than once in a subcycle along with zero vectors, there are multiple sequences are possible. Therefore, considering the simplicity and performance constraints following conditions must be satisfied by a sequence for a practical implementation.

1. The four active vectors (2M+2L) needs to be used in a subcycle at least once.
2. Either one of the zero vectors (0,32) needs to be used in a subcycle at least once.
3. If an active vector is applied more than once during a subcycle, the total amount of time the vector is applied must meet (1).
4. For a state transition, only one state needs to change.

The above condition ensures the volts-second balance and avoids unwanted switching.

Advanced Phase Clamp PWM (APCPWM) is classified into three different ways, termed as APCPWM_01$(M_a + L_b)$, APCPWM_02$(M_b + L_a)$ and APCPWM_03$(L_a + L_b)$ where, $M_a, M_b, L_a and\ L_b$ they are respective medium and large vectors. The proposed PWM techniques switching is delineated in Table 3.2 for sector 1.

Table 3.2: Advanced PWM Switching Sequences for Sector 01

Sr. No.	Proposed PWM Techniques	Switching sequence in sector 01
1	Clamp 36°_APCPWM_01	31,5,3,5,3,6,2,2,6,3,5,5,3,31
2	Clamp 36°_APCPWM_02	31,5,3,6,2,6,2,2,6,2,6,3,5,31
3	Clamp 36°_APCPWM_03	31,5,3,6,3,6,2,2,6,3,6,3,5,31
4	Clamp 18° _APCPWM_01	0,2,6,2,6,3,5,5,3,6,2,6,2,0
5	Clamp 18°_APCPWM_02	0,2,6,3,5,3,5,5,3,5,3,6,2,0
6	Clamp 18°_APCPWM_03	0,2,6,3,6,3,5,5,3,6,3,6,2,0

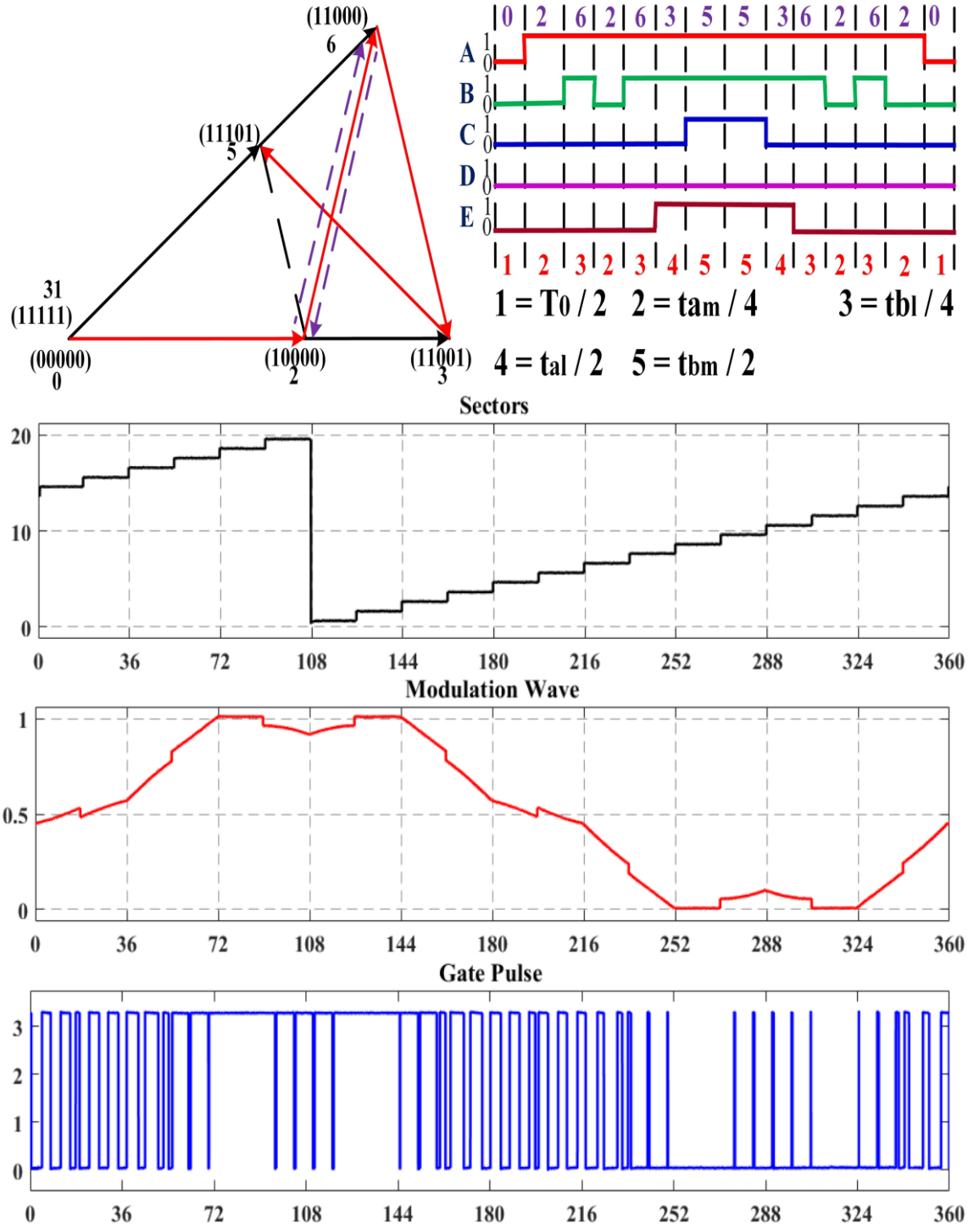

Figure 3.7. Clamp 18^0APCPWM 01 (On the Top Left Side-Space Vector Locations, On the Top right side-Gate pulses in the first sector, Bottom is having Sectors, Modulation Index, Gate Pulse of Clamp 18^0 APCPWM 01)

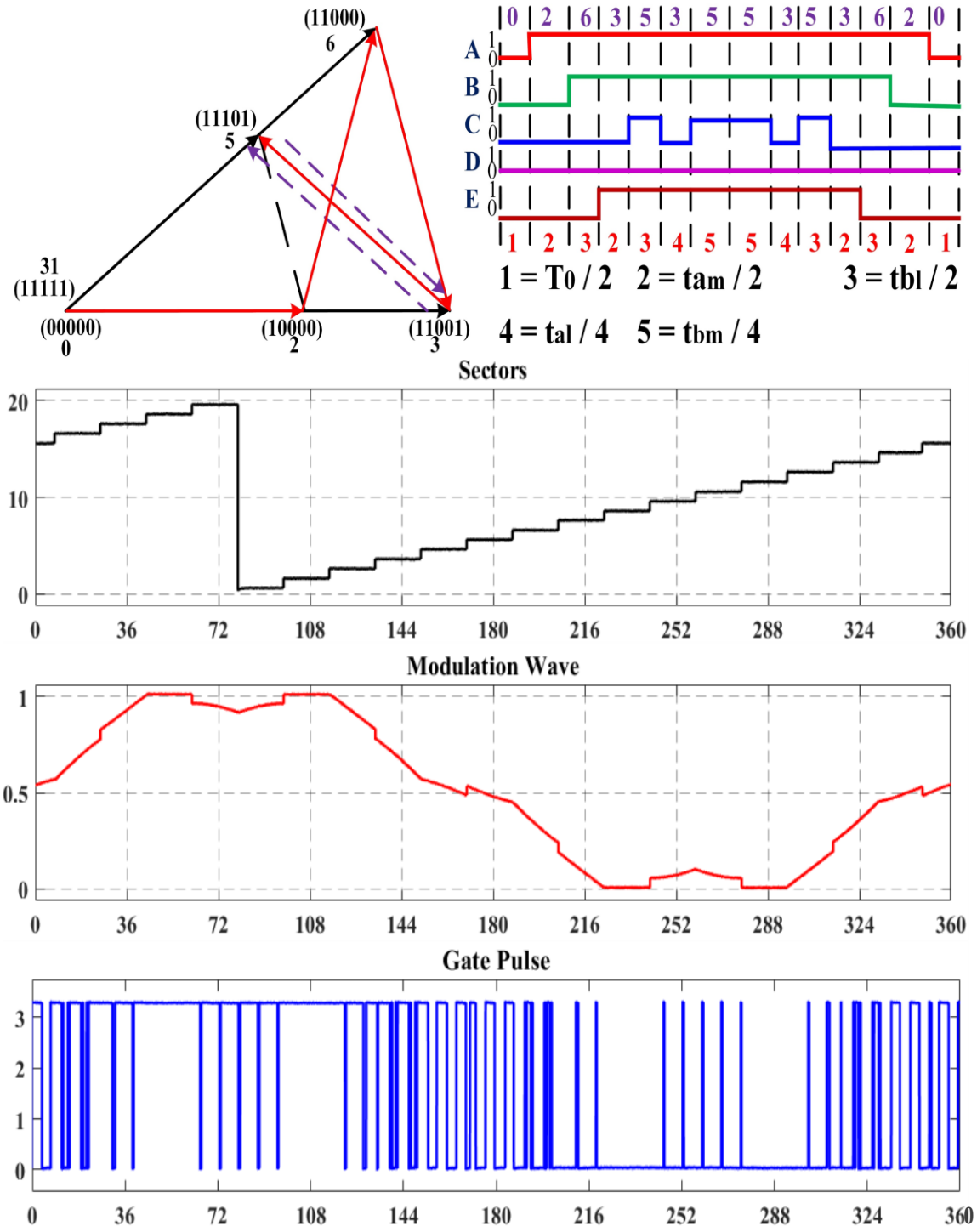

Figure 3.8. Clamp 18^0APCPWM 02 (On the Top Left Side-Space Vector Locations, On the Top right side-Gate pulses in the first sector, Bottom is having Sectors, Modulation Index, Gate Pulse of Clamp 18^0APCPWM 02)

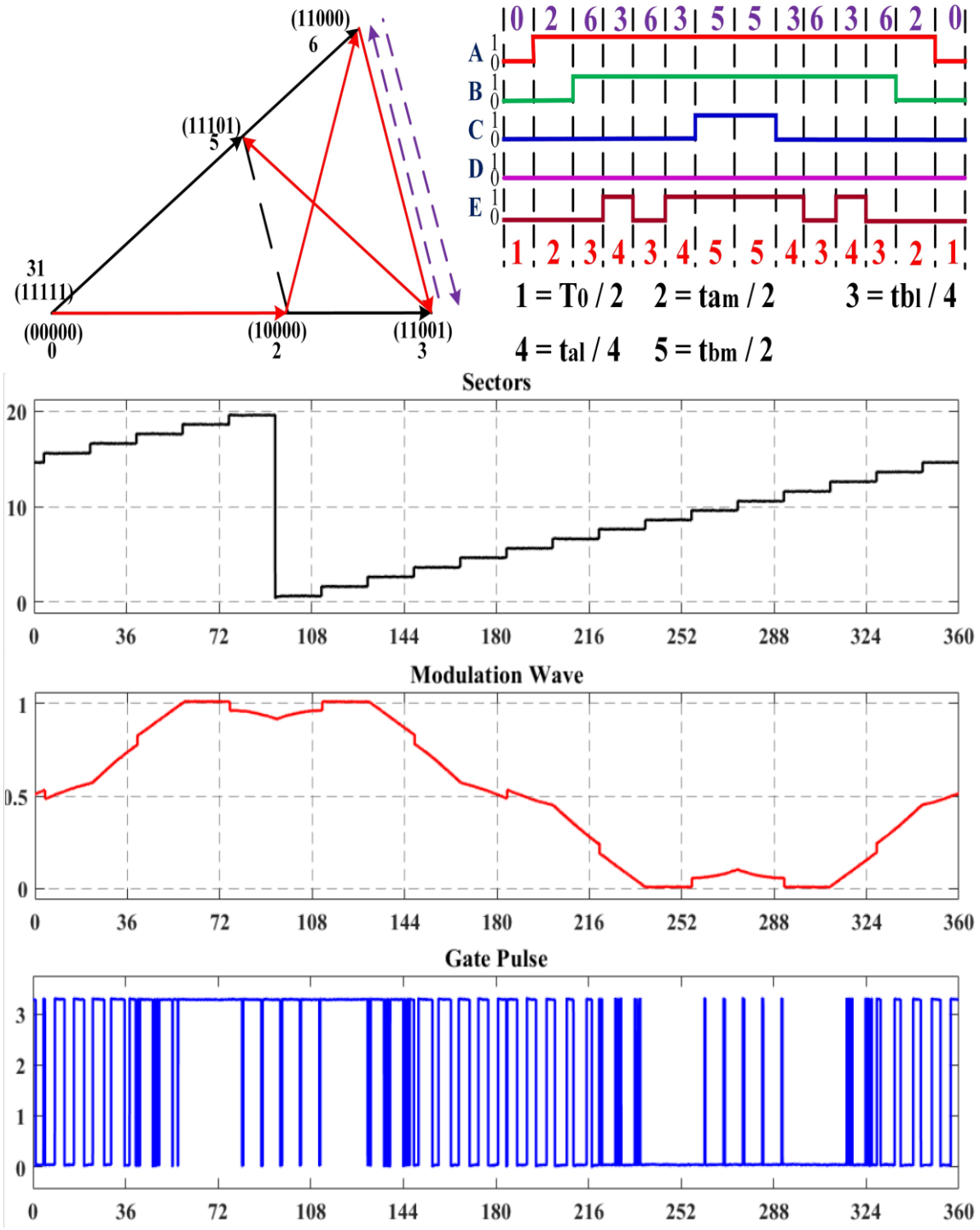

Figure 3.9. Clamp 18^0 APCPWM 03 (On the Top Left Side-Space Vector Locations, On the Top right side-Gate pulses in the first sector, Bottom is having Sectors, Modulation Index, Gate Pulse of Clamp 18^0APCPWM 03)

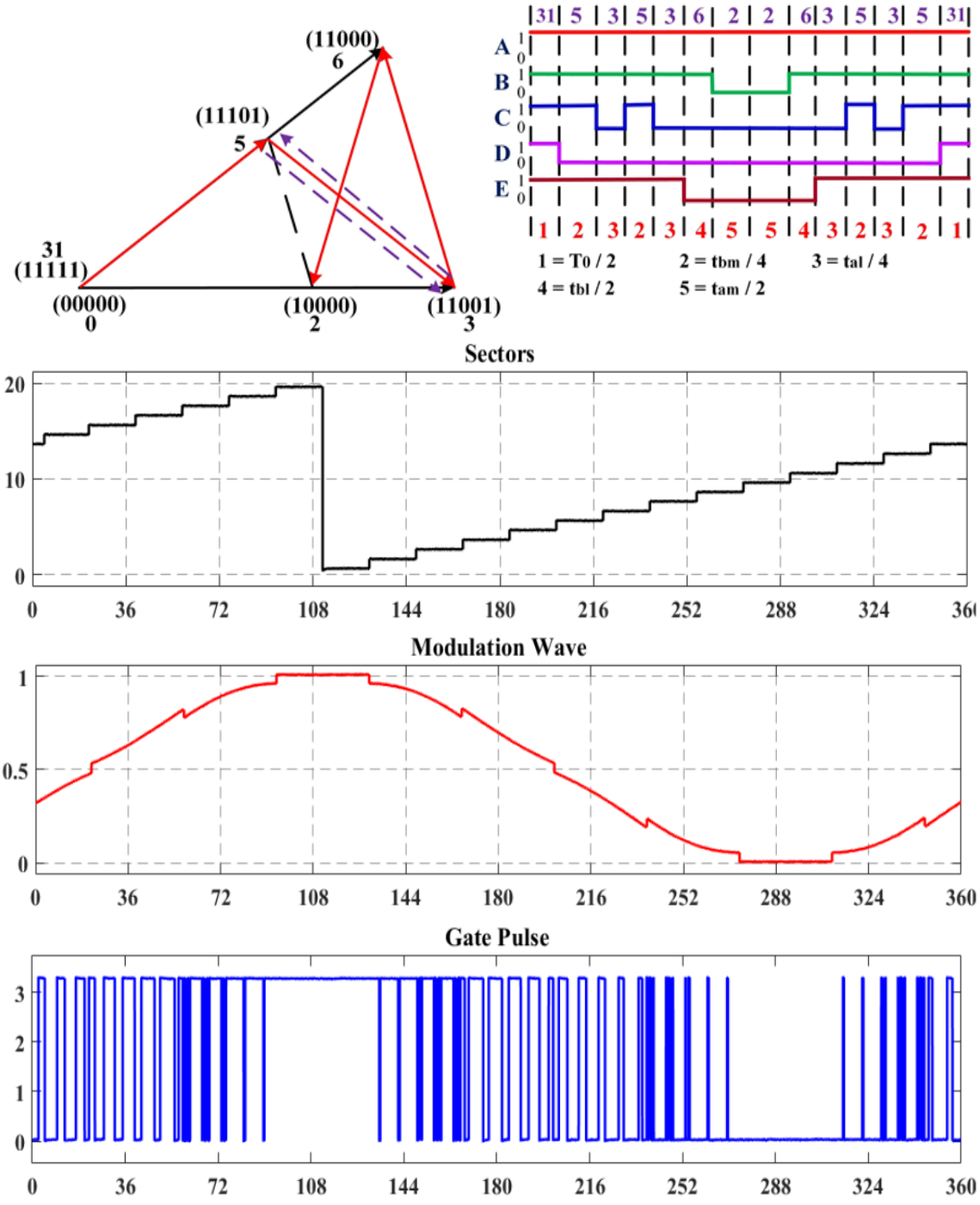

Figure 3.10. Clamp 36^0APCPWM 01 (On the Top Left Side-Space Vector Locations, On the Top right side-Gate pulses in the first sector, Bottom is having Sectors, Modulation Index, Gate Pulse of Clamp 36^0APCPWM 01)

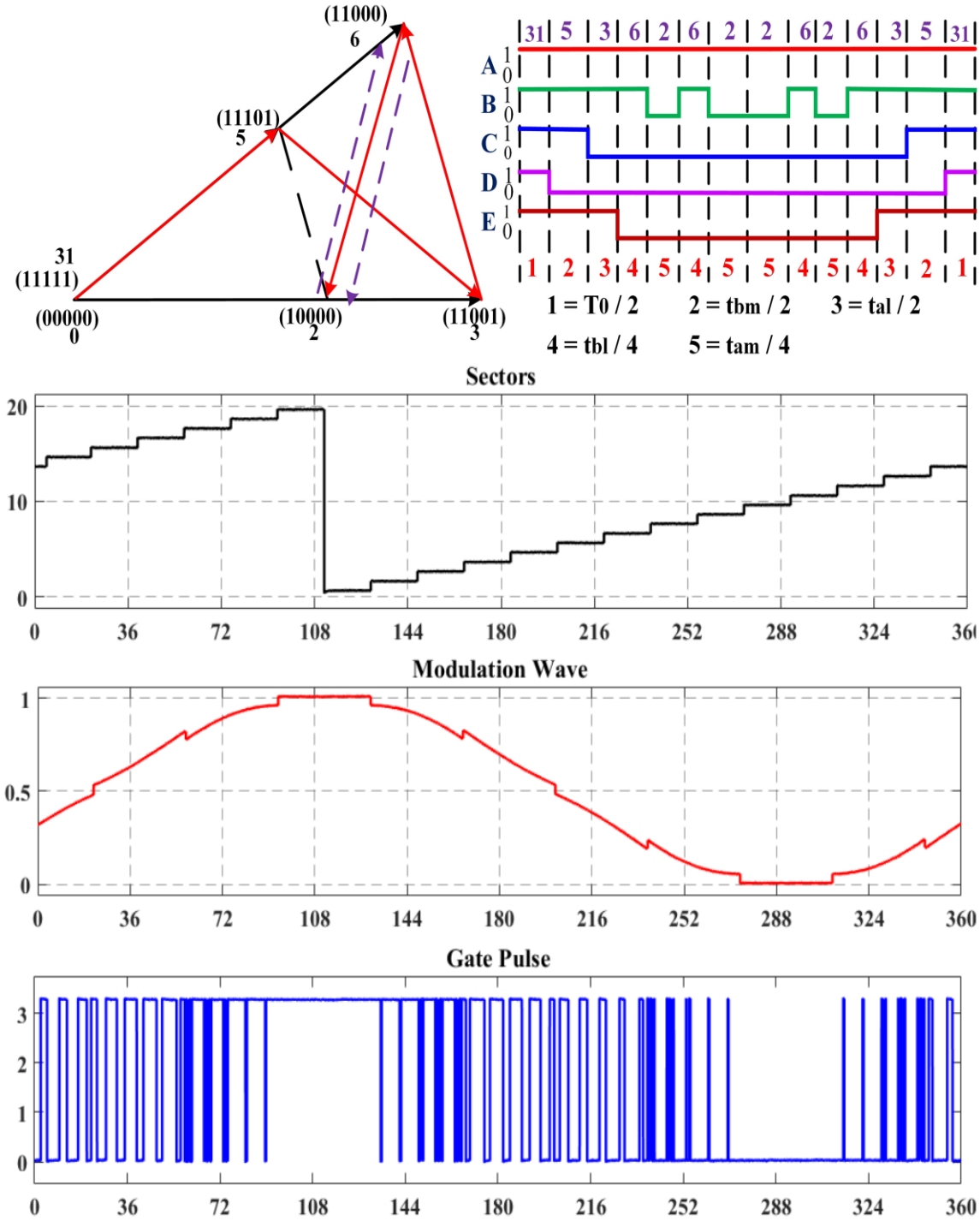

Figure 3.11. Clamp 36^0 APCPWM 02 (On the Top Left Side-Space Vector Locations, On the Top right side-Gate pulses in the first sector, Bottom is having Sectors, Modulation Index, Gate Pulse of Clamp 36^0 APCPWM 02)

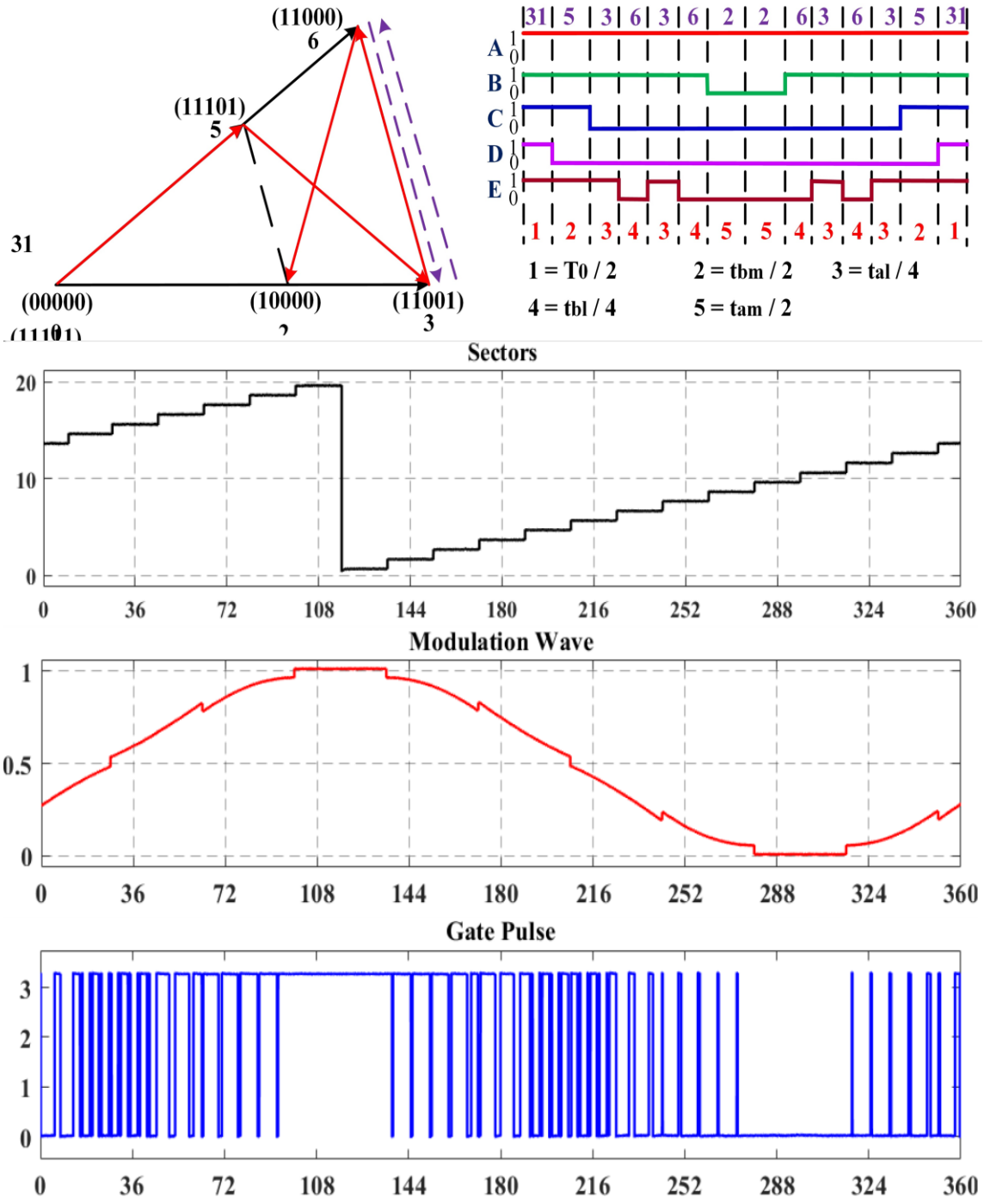

Figure 3.12. Clamp 36^0 APCPWM 03 (On the Top Left Side-Space Vector Locations, On the Top right side-Gate pulses in the first sector, Bottom is having Sectors, Modulation Index, Gate Pulse of Clamp 36^0APCPWM 03)

CHAPTER 4

RIPPLE CURRENT ANALYSIS IN MULTIPHASE DRIVE

The complex space vector approach, which is already used in the evaluation of the continuous and discontinuous PWM techniques, is used in the current ripple analysis, as was previously described., and is based on the flux HDF approach in [30]– [33]. The time integral of the harmonic voltage vector, or the voltage vector produced during the creation of the output voltage reference vector, is represented by the harmonic flux. The complex space vector approach allows for multi-step analysis and offers great insight into the mechanism of output current ripple creation This enables the harmonic flux trajectories in each of the two planes over a switching period to be visually represented initially. The squared harmonic flux rms is then calculated, and it varies for every modulation scheme. Finally, the flux HDF of each plane is computed, which is obtained from the integrated squared harmonic flux throughout the fundamental period. A brief discussion of the procedure in [30],[31] and its relevance to Advanced Phase Clamp PWM techniques is given.

4.1. Creation of Ripple in Output Current

There is always a difference between the applied voltage vector and the reference vector since the inverter is discrete. Current ripple will occur when this output voltage variation is applied across the load.

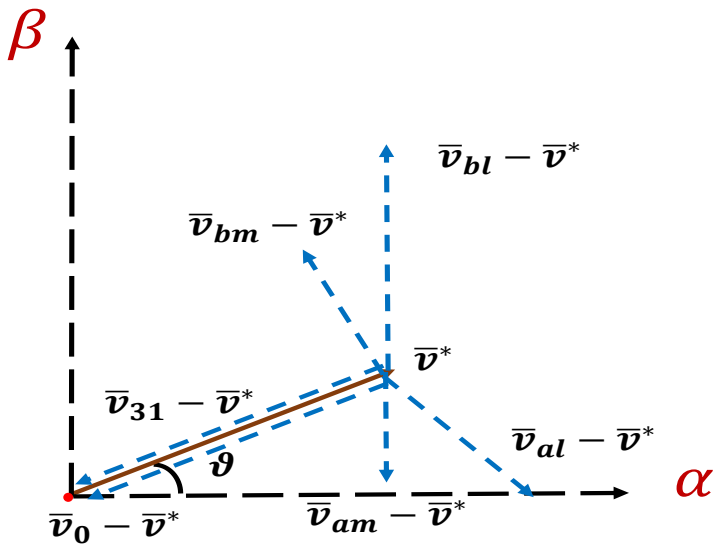

Fig. 4.1. error voltage generation

The analytical model can be made simpler into

$$\bar{v}_{error} = \bar{v} - \bar{v}^* \tag{4.1}$$

$$\Delta\bar{\imath} = \frac{\bar{v} - \bar{v}^*}{L_\sigma} \Delta t \tag{4.2}$$

where $\bar{v}$ is the reference voltage vector,$\bar{v}^*$ is the space vector active across the time interval Δt inside a switching period, and L_σ is the equivalent inductance for the switching harmonics. Since it is more difficult to prove this equivalent inductance in multiphase systems [31], [32] than in three-phase systems, the idea of the harmonic flux $\Delta\bar{\lambda}$ [25] is used.

$$\Delta\bar{\lambda} = L_\sigma \Delta\bar{\imath} = (\bar{v} - \bar{v}^*)\Delta t \tag{4.3}$$

4.1.1 Steps Followed for the Ripple Current Analysis

The flux HDF technique is now the foundation of the current ripple analysis. It makes use of the complex space vector technique, which enables the following steps to be taken in the analysis:

1. Graphical illustration of the harmonic flux trajectories in both planes throughout a switching period.
2. Calculation of squared harmonic flux rms over every modulation index.
3. Total HDF (Harmonic Distortion Factor) across the fundamental period

4.1.1.1 Harmonic Flux Trajectories

The error voltage vector's trajectories in both planes throughout the switching time are known as the harmonic flux trajectories. Because of the symmetry, the harmonic flux deviations are computed at the conclusion of each half interval during the first half of the switching period

This idea enables a separate analysis of the harmonic flow in each plane. Assuming a zero initial value for the harmonic flux deviation, all SVPWM schemes (CSVPWM, BCPWM, and Advanced PWM) can generate harmonic flux trajectories (trajectories of error voltage vectors) in both planes during the switching period based on (4.3). As in [30]

and [33], Due to the symmetrical switching pattern, variations of the harmonic flux can be obtained by taking into account only half of the switching period.

$$\Delta\lambda_N = L\Delta i_N = \frac{V_{dc}T_s}{8} \tag{4.4}$$

Each plane can now be subjected to expression (4.5) while maintaining the applied vectors' sequence Since the order varies for sophisticated PWM systems and different sequence orders are used in the odd and even sectors, the applied active vectors are designated I through VI to accommodate for the general case. [31] provides the harmonic flux trajectory value after each half interval.

$$\begin{aligned}
&\Delta\bar{\lambda}(0) = 0 \\
&\Delta\lambda(\mathrm{t}_1) = -t_0\bar{v}^* \\
&\Delta\lambda(t_2) = \Delta\lambda(\mathrm{t}_1) + t_I(\bar{v}_I - \bar{v}^*) \\
&\Delta\lambda(t_3) = \Delta\lambda(\mathrm{t}_2) + t_{II}(\bar{v}_{II} - \bar{v}^*) \\
&\Delta\lambda(t_4) = \Delta\lambda(\mathrm{t}_3) + t_{III}(\bar{v}_{III} - \bar{v}^*) \\
&\Delta\lambda(t_5) = \Delta\lambda(\mathrm{t}_4) + t_{IV}(\bar{v}_{IV} - \bar{v}^*) \\
&\Delta\lambda(t_6) = \Delta\lambda(\mathrm{t}_5) + t_V\,(\bar{v}_V - \bar{v}^*) \\
&\Delta\lambda(t_7) = \Delta\lambda(\mathrm{t}_6) + t_{VI}(\bar{v}_{VI} - \bar{v}^*)
\end{aligned} \tag{4.5}$$

Plotting the applied vectors' harmonic flux trajectories throughout a sub-cycle with $m = 0.75$ and $\theta = 0°, 12°, 24°$ and $36°$ are shown in Fig.4.2-Fig.4.5. to emphasize the following important facts:

1. Since the $x_3 - y_3$ plane represents the third harmonic components and the $\alpha - \beta$ plane contains the fundamental components, the harmonic flux trajectories in the two planes are distinct [35].
2. In Clamp $18°$ and Clamp $36°$, as there are a total of 20 sectors of $18°$ each and in CSVPWM, there are a total of 10 sectors of $36°$ each. Because of the different vector sequences applied with respect to odd and even sectors, the harmonic flux trajectories in $\alpha - \beta$ plane and $x_3 - y_3$ plane possess the same nature of trajectories for θ equal to $12°$ and the different nature of trajectories for θ equal to $24°$ which is actually following the second sector sequence as per CSVPWM.

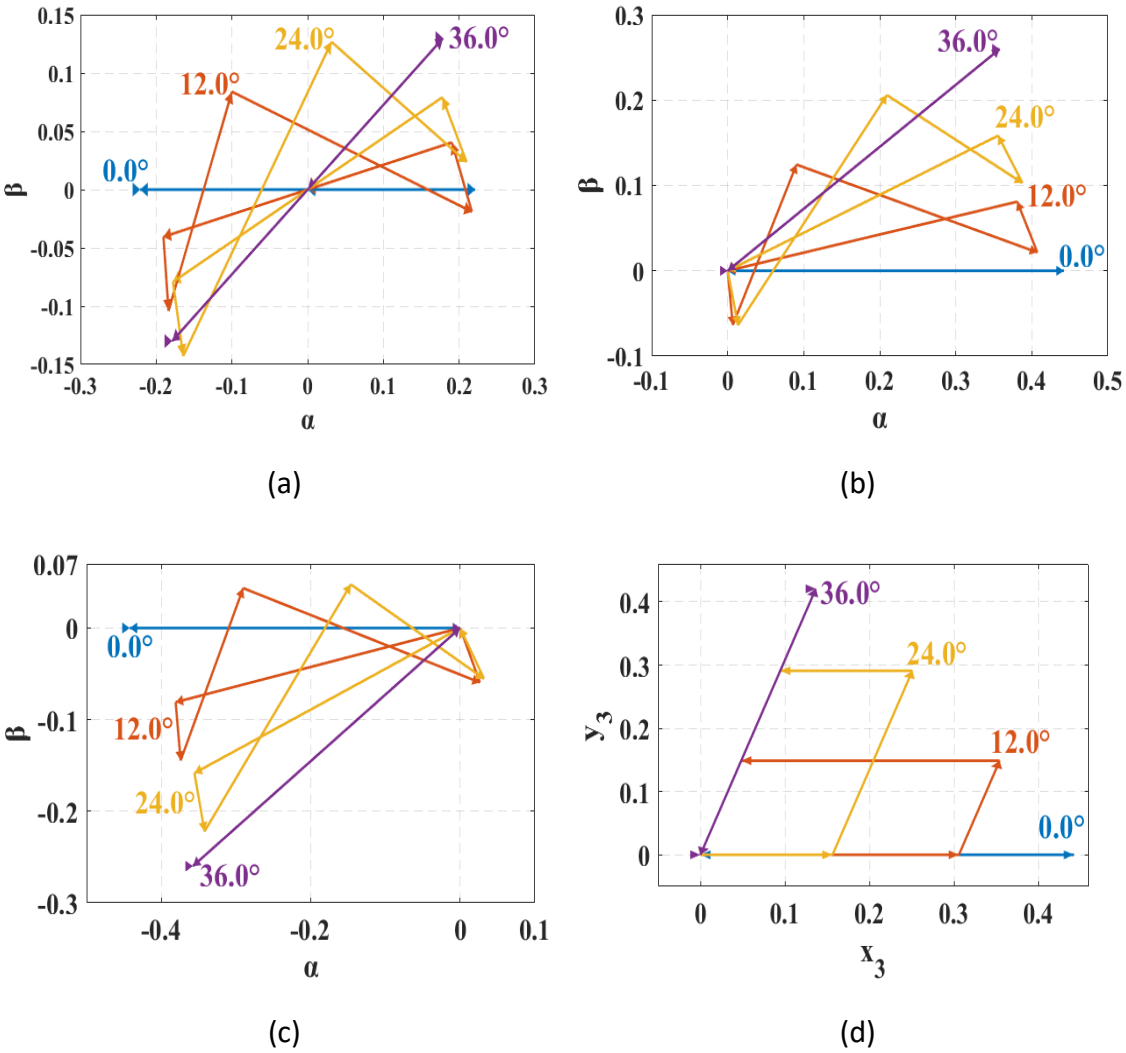

Fig. 4.2 Harmonic flux trajectories for *m* = 0.75 across a sub-cycle (Ts/2) (a)CSVPWM (b) 72^0 Negative Clamp (c)72^0 Negative Clamp in $\alpha - \beta$ plane (d) above PWM in $x_3 - y_3$ plane

3. Because of these the relative error between the reference vector$(\bar{v}^*)$ and the space vectors following the applied sequence for $\theta > 18°$ shows minimum and maximum error for Clamp 36° and Clamp 18° respectively which further results into the harmonic content of PWM techniques Fig 4.2(d) & Fig 4.5(a).
4. In contrast to BCPWMs, the CSVPWM has equal zero state partitioning. This indicates that the harmonic flux trajectories over the $\alpha - \beta$ plane for CSVPWM will be symmetrical to the origin for a given angle (θ), but not for BCPWMs. (Fig.4.2 (a), (b), (c)).

5. As assuming the eccentricity of harmonic flux initially to be zero, returning the trajectories at the same locus at the end of every half interval ensures the volt-second balance of the corresponding switching

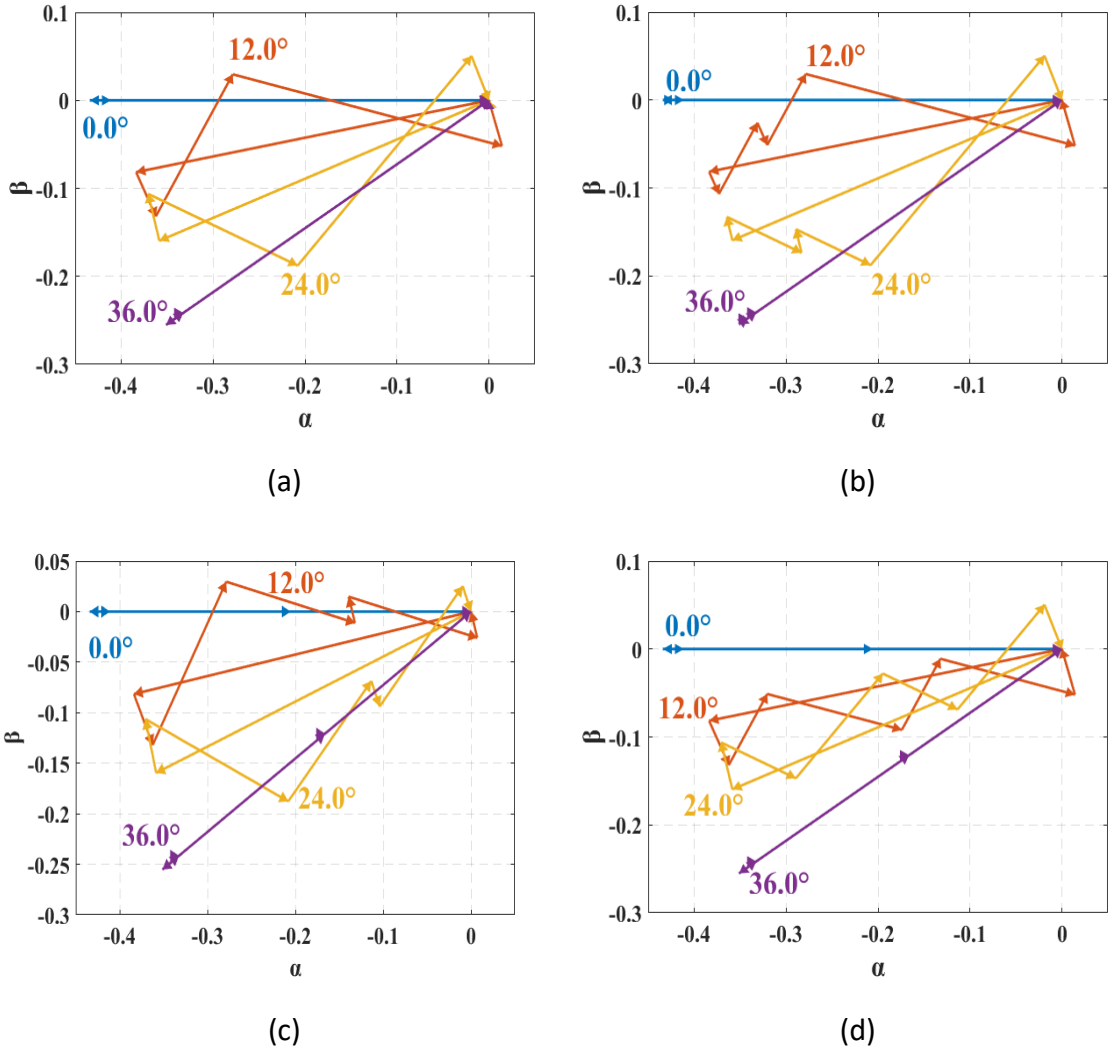

Fig. 4.3 Harmonic flux trajectories for m = 0.75 across a sub-cycle (Ts/2) in $\alpha - \beta$ plane (a)Clamp 18° (b) Clamp 18° _APCPWM_01(c)Clamp 18° _APCPWM_02 (d) Clamp 18° _APCPWM_03

6. Harmonic flux trajectories in the $x_3 - y_3$ plane are solely a function of active space vectors, as mentioned in [21], and not of zero space vectors. Thus, as can be shown in Fig. 4.3 and Fig 4.4, the harmonic flux trajectories of both BCPWM techniques are identical. because zero state partitioning is the basis for the differences amongst BCPWM approaches.
7. In contrast, APCPWM techniques use active space vector partitioning, which is why APCPWM_01, APCPWM_02, and APCPWM_3 all have distinct harmonic

flux trajectories in the $x_3 - y_3$ plane. Space vector partitioning, which is why APCPWM_01, APCPWM_02, and APCPWM_3 all have distinct harmonic flux trajectories in the $x_3 - y_3$ plane.

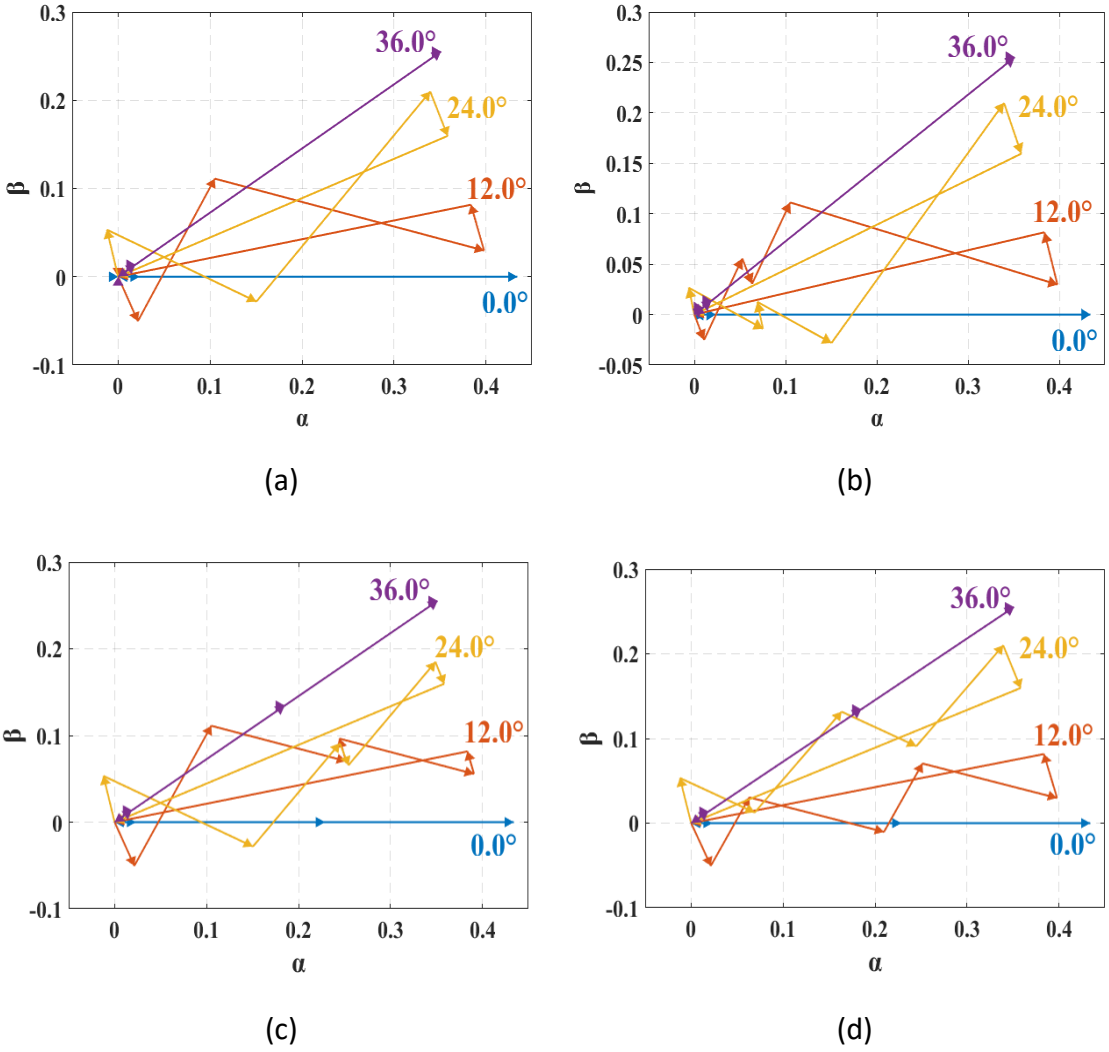

Fig. 4.4 Harmonic flux trajectories for m = 0.75 acrossa sub-cycle (Ts/2) in $\alpha - \beta$ plane (a)Clamp 36° (b) Clamp 36° _APCPWM_01(c)Clamp 36° _APCPWM_02 (d) Clamp 36° _APCPWM_03

8. The application of a same active vector twice in a sub-cycle, reduces the peak magnitude of the harmonic flux trajectories which further results into the reduction of overall phase current THD.
9. The reduction in peak magnitude of harmonic flux trajectories is same in the case of APCPWM_01 and APCPWM_02 as both techniques are employing the medium and large active vector twice in a sub cycle. Fig. 4.3 and Fig 4.4.

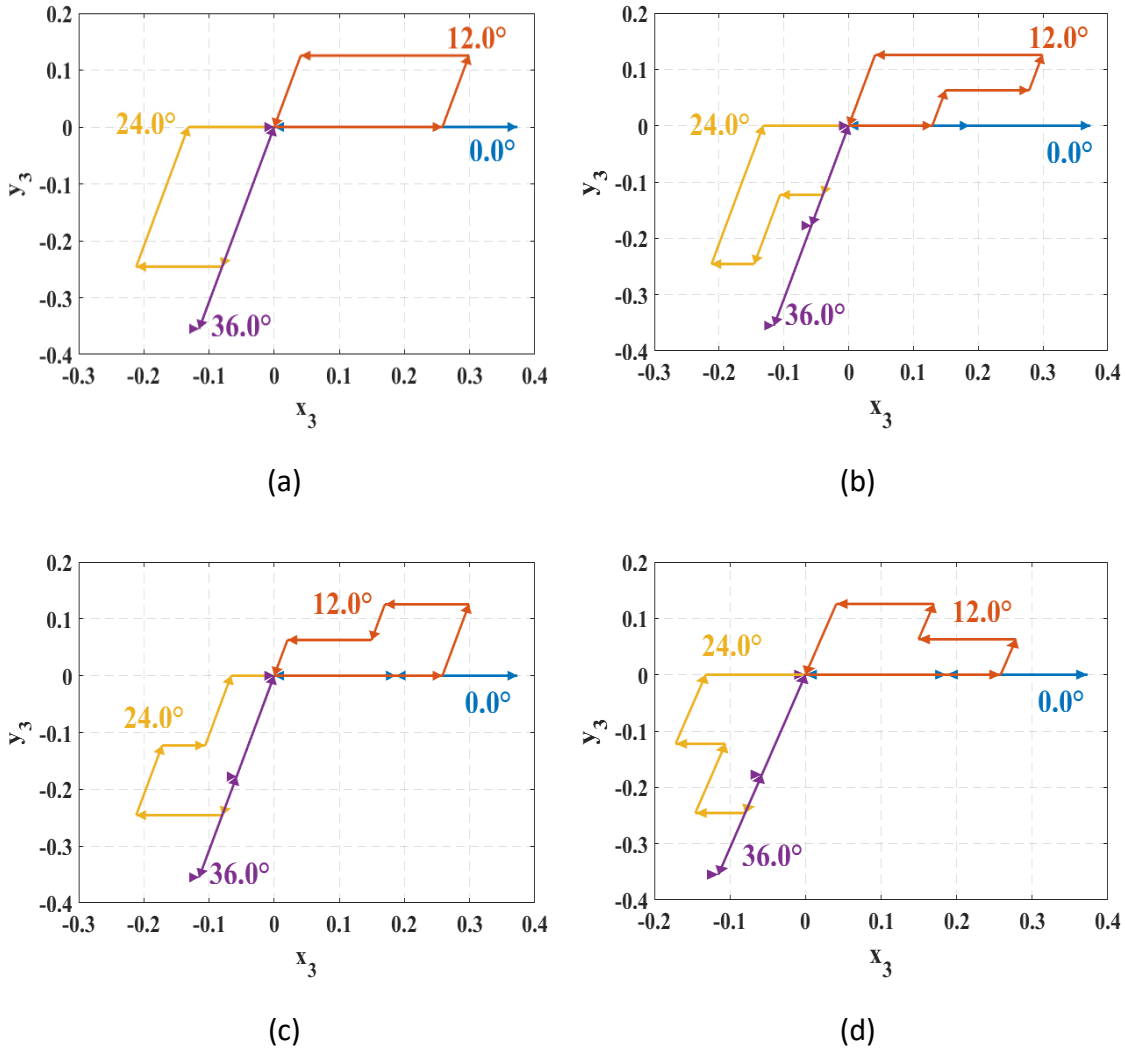

Fig. 4.5 Harmonic flux trajectories for m = 0.75 across a sub-cycle (Ts/2) over $x_3 - y_3$ plane (a)both for CSVPWM and BCPWM (b) APCPWM_01(c)APCPWM_02 (d) APCPWM_03

10. The maximum reduction of nearly 50% in peak magnitude of the harmonic flux trajectories is observed in the case of APCPWM_03, as it employs the two large active vectors twice in a sub-cycle Fig. 4.3(d) and Fig 4.4.(d).

4.1.1.2 Evaluation of Squared Harmonic Flux

The average squared value of the harmonic flux is used as a figure of merit since the second step involves analysing the harmonic flux over the switching period. Only $T_s/2$ needs to be calculated because the trajectories' first and second halves have the same rms value due to symmetry. The following integral must be solved:

$$\Delta\lambda^2_{abcde-RMS} = \frac{2}{T_s}\int_0^{\frac{T_s}{2}} \Delta\lambda^2_{abcde}\, dt \tag{4.6}$$

The entire five-phase system solution is achieved by representing all five phases on the left-hand side of equation (4.6). Since the harmonic flux eccentricities in each of the two 2-D planes may be linked to the quantity $\Delta\lambda^2_{abcde}$ [30], (4.6) adopts the following form.

$$\begin{aligned}\Delta\lambda^2_{abcde-RMS} &= \Delta\lambda^2_{abcde-RMS\alpha\beta} + \Delta\lambda^2_{abcde-RMSxy} \\ &= \frac{5}{2}\frac{2}{T_s}\left[\int_0^{\frac{T_s}{2}} \left[\Delta\lambda^2_\alpha + \Delta\lambda^2_\beta\right]dt + \int_0^{\frac{T_s}{2}} \left[\Delta\lambda^2_\alpha + \Delta\lambda^2_\beta\right]dt \right]\end{aligned} \tag{4.7}$$

Based on the existing half intervals, expression (4.7) can be separated into multiple integrals. Subsequently, by utilizing the method outlined in [30], a broadly applicable solution for each of the 2-D planes can be derived, which is assessed mathematically. The features of the squared harmonic flux of the APCPWM techniques analysed in this paper are plotted for two sectors shown in Figs.4.6 and Fig.4.7. which would be same for all the 20 sectors It can be seen that every modulation method has a unique and different characteristic in the $\alpha - \beta$ plane as well as in $x_3 - y_3$ plane also.

A. <u>$\alpha - \beta$ plane:</u>

1. Around m = 0.6, the value peaks, after which it falls as the modulation index rises for all the PWM methods. For BCPWM the squared harmonic flux rms values are quite similar in magnitude at higher modulation index.
2. The APCPWMs possess the identical shape as that of BCPWM with slight reduction in magnitude

B. <u>$x_3 - y_3$ plane</u>

1. The plots in the $x_3 - y_3$ planes are only a function of active state portioning and do not depend upon the zero space vectors. Therefore, the plots for CSVPWM and BCPWMs are the same.
2. The changes are observed in APCPWM techniques prominently at higher modulation index, indicating its angular position dependencies Fig 4.7 a reduction in magnitude of squared harmonic flux in the order of (CSVPWM, BCPWM) > (APCPWM_01, APCPWM_02) > APCPWM_03.

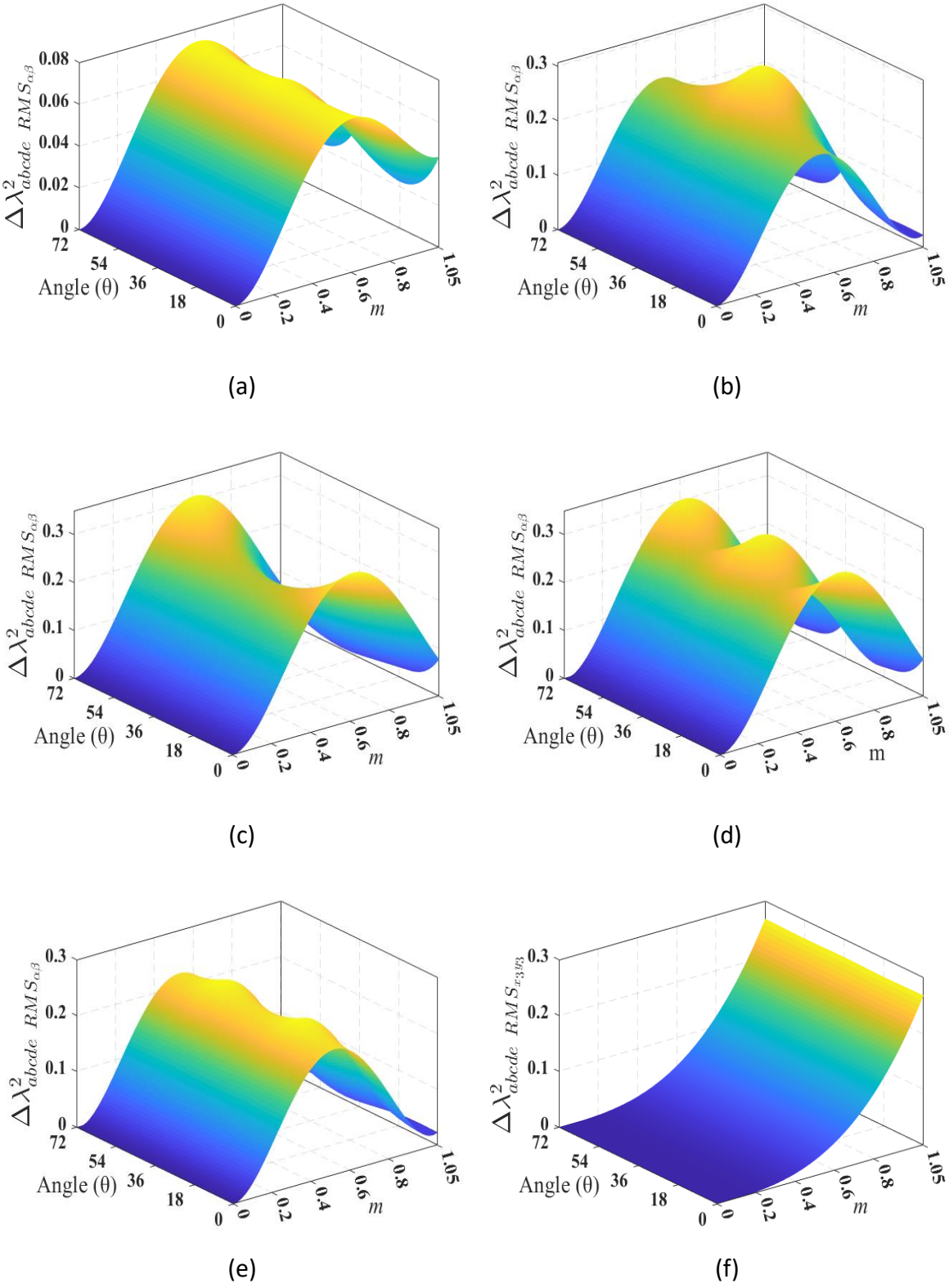

Fig. 4.6 Squared Harmonic flux over $\alpha - \beta$ plane for (a) CSVPWM (b) (b)72^0 Positive Clamp (c)72^0 Negative Clamp (d)Clamp 18^0 (d)36^0Clamp (e) Squared Harmonic flux over $x_3 - y_3$ plane for CSVPWM and BCPWM techniques

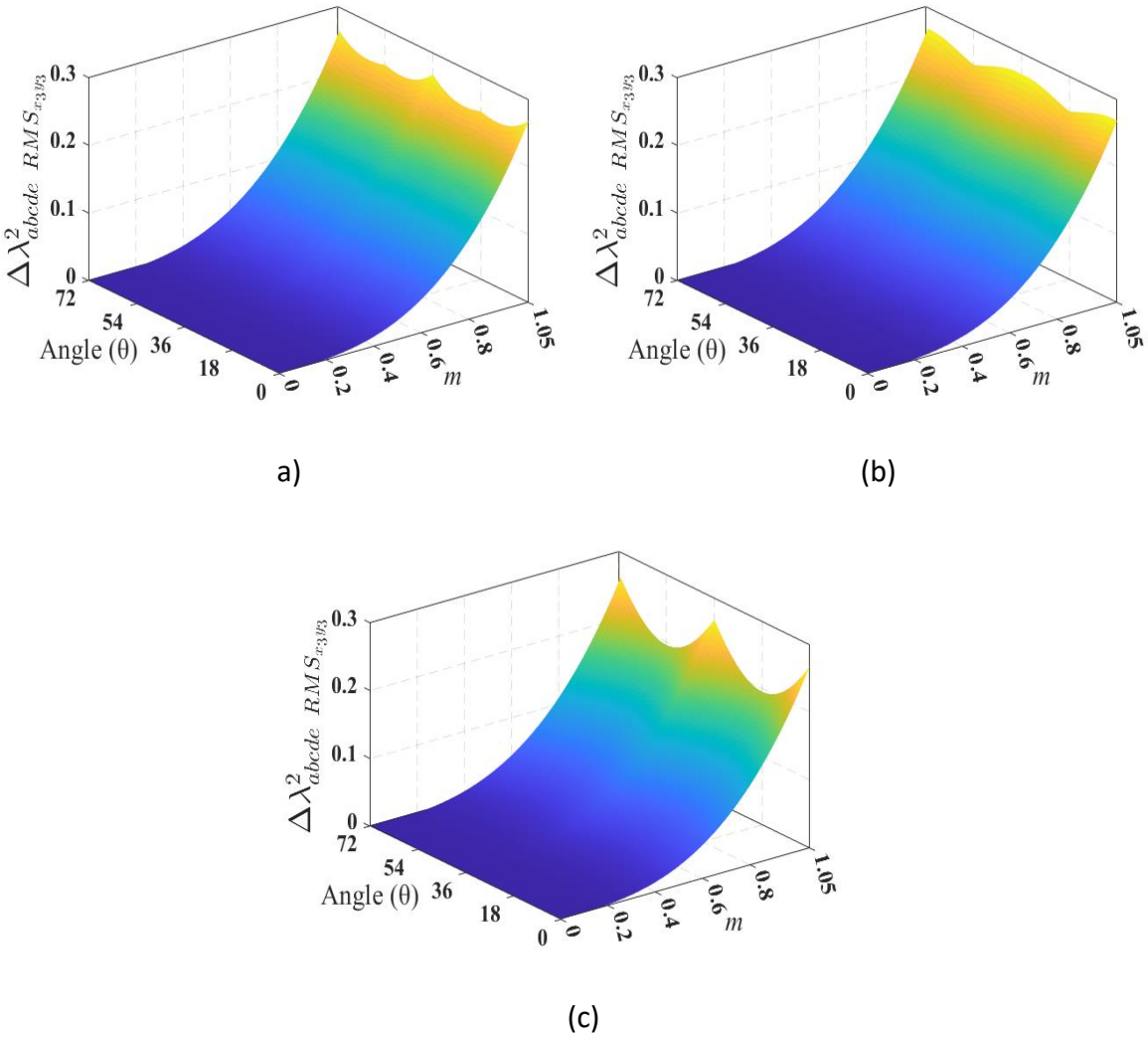

Fig. 4.7 Squared harmonic flux in $x_3 - y_3$ plane (a) APCPWM_01 (b) APCPWM_02 (c) APCPWM_03

3. Fig. 4.8 shows a cross-sectional view of Fig. 4.7 and Fig. 4.6 (at m=1.0), revealing the squared harmonic flux as a strong function of angular position in $x_3 - y_3$ plane. APCPWM, unlike the CSVPWM and BCPWMs.
4. The minimum rms flux is observed $\theta = 18°$ in APCPWM_03, which employs both large vectors $(L_a + L_b)$ twice in a sequence.
5. Analysing the Fig.4.8, Its relationship between different zones and curves it can be expected that the APCPWM_03 will have the least current harmonic content as compared to other PWM techniques.

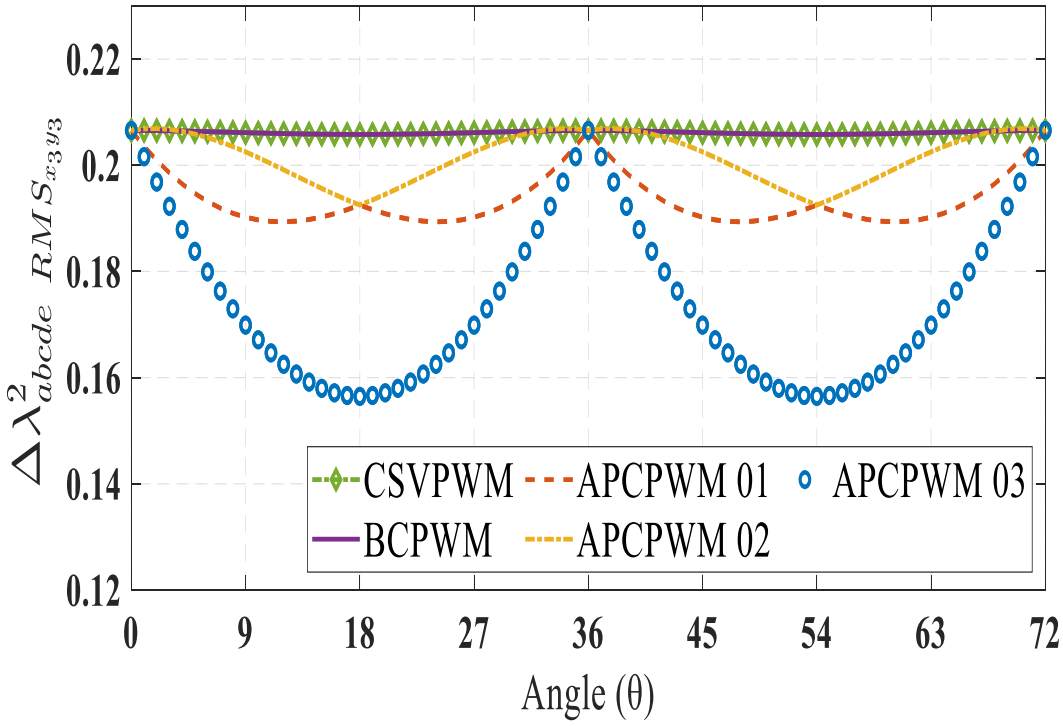

Fig.4.8. Squared harmonic flux at m = 1.0 in $x_3 - y_3$ plane of CSVPWM, BCPWM and advanced PWM Techniques

4.1.1.3 Flux HDF Analysis

Finally, to generate flux HDFs in each plane, the squared harmonic flux needs to be integrated across the fundamental period. For the same reasons as before, the integration should be implemented across the first two sectors, including

$$\Delta\lambda^2_{abcde-RMSF} = \frac{5}{2\pi}\int_0^{\frac{2\pi}{5}} \Delta\lambda^2_{abcde-RMS}\, d\theta \tag{4.8}$$

It is not always simple to define the polynomial closed-form solution of (4.7) in a short and compact form, as [30] and [31] show. Therefore, the numerical integration of (4.8) in MATLAB is used to derive the HDFs of the modulation methods that are being analysed.

Compared to the equivalent BCPWMs and APCPWMs, the CSVPWM has a reduced HDF in the $\alpha - \beta$ plane.

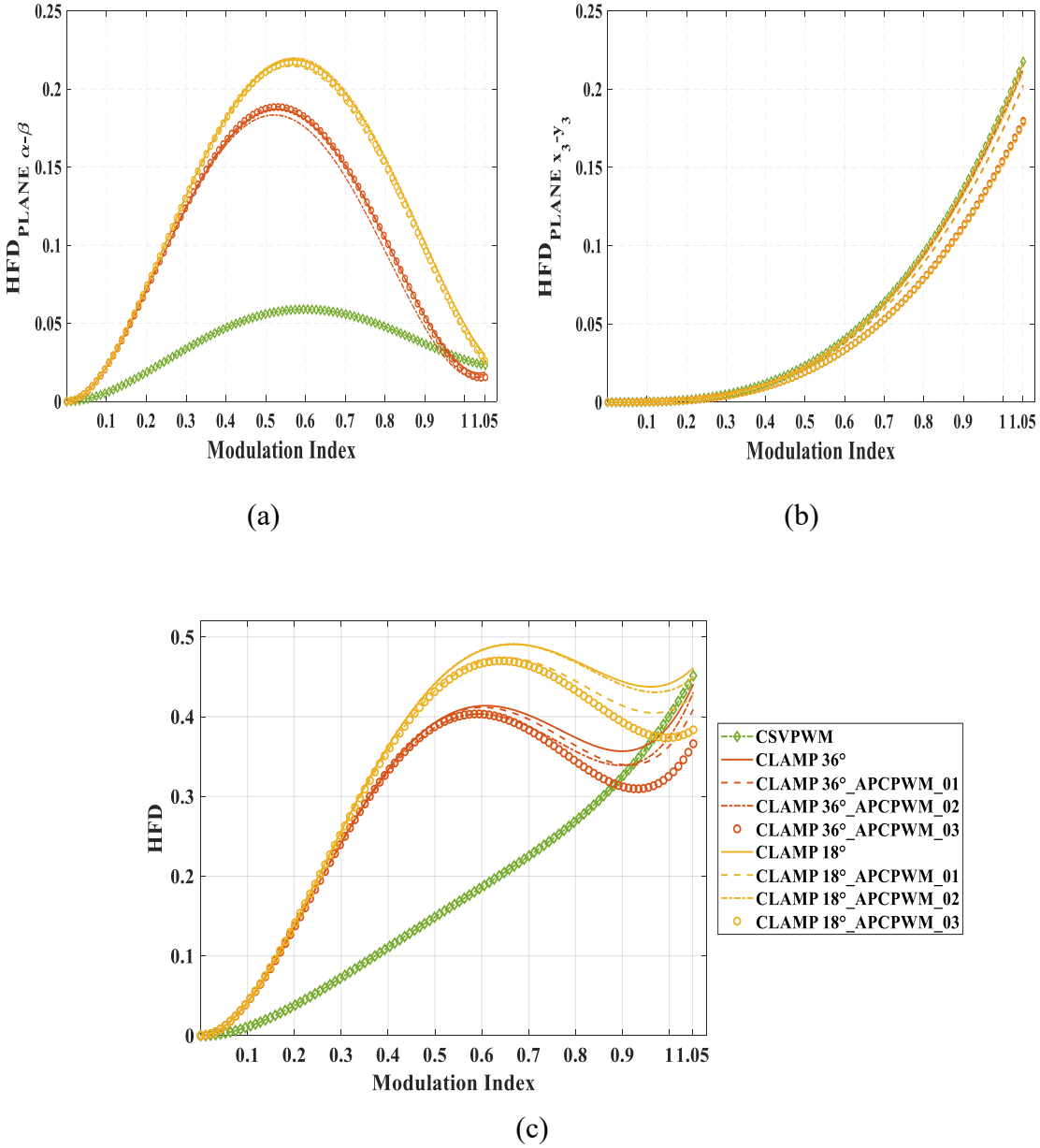

Fig. 4.9.HDF curves show the range of the feasible modulation indices for every PWM technique that was examined

For advanced bus clamping modulation approaches at the same switching frequency, these HDFs are displayed in Fig. 4.9. Regarding HDF behaviour, the following is applicable.

1. The magnitude of APCPWMs is somewhat smaller than that of equivalent BCPWMs.
2. The rms flux HDF depicted in Fig. 4.9 (b) is significantly reduced in the case of ADPWMs approaches. The APCPWMs outperform both CSVPWMs and

BCPWMs in the high modulation index range. APCPWM_03 shows the maximum reduction in the flux HDF followed by APCPWM_01 and APCPWM_02 respectively.

3. Note that as the modulation index rises, the $x_3 - y_3$ plane's influence becomes more noticeable. Because the HDFs of the first plane, which contains harmonics of the order 10k±1, somewhat change the properties of the second plane, which represents harmonics of the order 10k±3, the mutual relationship between the HDFs of each scheme is preserved as illustrated in Fig. 4.9 (c). The $x_3 - y_3$ plane dominates the final HDF characteristics.
4. At higher modulation index (for modulation index greater than 0.9) 36°_APCPWM_03 is better than PWM techniques including CSVPWM showing least current harmonic content with a significant reduction in flux HDF. This supports the claims made in the sections before this one, where the harmonic flux was examined.

.

CHAPTER 5

EXPERIMENTAL ANALYSIS AND DSP-BASED IMPLEMENTATION OF PWM TECHNIQUES

5.1. Real-time Implementation of PWM Algorithm using DSP TMS320F28379D

5.1.1 Introduction

Implementation of various sophisticated PWM algorithms for continuous and discontinuous PWM techniques, including sine triangle comparison or space vector-based PWM techniques, is made possible by DSP. A selected few DSPs, including the TMS320F2812, TMS320F28335, and TMS320F28379D, were created specifically for use in electric drive applications. They are extensively utilized in numerous fields, including robotics, electric vehicles, industrial automation, and others.

There are different types of peripherals with their frequencies in DSP 28379D for motor control:

1. GPIOs (General purpose input output)
2. ePWM (Enhanced pulse width modulator) module
3. ADC (Analog to Digital converter) and DAC (Digital to Analog Converter)
4. eQEP (Enhanced quadrature encoder pulse)

5.1.2 GPIOs (General Purpose Input Output Pins)

Depending on the direction indicated by the (DIR) direction registers, the pins that are chosen can be used as both input and output. To make sure there is no voltage on the designated pin, pull-up registers are utilized to disable pull-up resistance. Data (DAT) registers are used to set, clear, and toggle the pin to determine how long it takes the controller to perform the main function.

1. GPyDAT Registers.

2. GPyPUD Registers
3. GPyDIR Registers.

5.1.3 ePWM (Enhanced Pulse Width Modulator) Module

Utilizing compare registers, this module is specifically intended to adjust the output voltage and frequency. The time-based counter is used to set the time-based period (TBCTR) value for comparison to create the pulses. The compare value (CMPA/B) and time-based period (TBPRD) can be changed, which will alter the pulse frequency. Additionally, to prevent short circuits between the power electronic switches in the VSI, this module offers a dead band or blanking time

1. CMPx Registers
2. TBPRD Registers
3. DBRED/DBFED Registers.

5.1.4 ADC (Analog to Digital Converter) and DAC (Digital to Analog Converter)

Both voltage and current are measured using voltage and current sensors. Signal conditioning circuits are used to transform the high voltages and currents into values between 0 and 3.3 volts. and then passed through an ADC into the DSP. The continuous signal is discretized, or sampled, according to sampling frequency. For subsequent processing, the digital findings are saved in ADC registers (AdcaResultRegs) continuously.

1. ADC_REGS Registers
2. ADC_RESULT_REGS Registers
3. ADCRESULTx Registers

The DAC transforms digital to analogue in order to display the discretized signal and can also be used to create other waves such as sine, triangle and square waves. It’s highly useful in verification and error detection within the algorithm. The DAC can accept the maximum value of 4095 (3.3-reference voltage). The value of the reference voltage can be modified using the DACREFSEL register.

1. DACVALA Registers
2. DACOUTEN Registers
3. DACREFSEL Registers

5.1.5 Flowchart Description of PWM Implementation

The flowchart given in Fig. 5.1 presents a real-time algorithmic sequence for implementing PWM signal generation using a Digital Signal Processor (DSP) in embedded power electronics applications.

The process begins by reading the modulation index and switching frequency, two critical parameters that govern the timing and amplitude of the generated PWM signals. Subsequently, the DSP is initialized by configuring essential hardware components, enabling clock systems, and setting up memory and peripheral registers.

The timer module, which forms the time base for PWM generation, is then configured along with its period interrupt to enable precise control loop execution. Once initialization is complete, the system enters the main control loop. Here, for every sampling instance, the reference voltage vector is computed based on desired output voltage conditions.

After identifying the corresponding sector in the space vector hexagon using this vector, the duty cycles for the inverter legs are calculated. For computational efficiency, the right switching vector is then chosen from a predetermined Lookup Table Unit (LUT).

The system subsequently monitors the occurrence of a timer period interrupt, which acts as a synchronization trigger. Upon the interrupt, the newly computed duty cycle values are loaded into the compare registers of the PWM module, effectively updating the output waveform in real time.

The interrupt flag is then cleared to allow the next interrupt event, and the system acquires the next set of control inputs or samples, thereby preparing for the subsequent iteration. This interrupt-driven, looped execution ensures precise timing, low latency, and deterministic behaviour, making it ideal for high-performance applications such as motor control, inverter modulation, or real-time power converters.

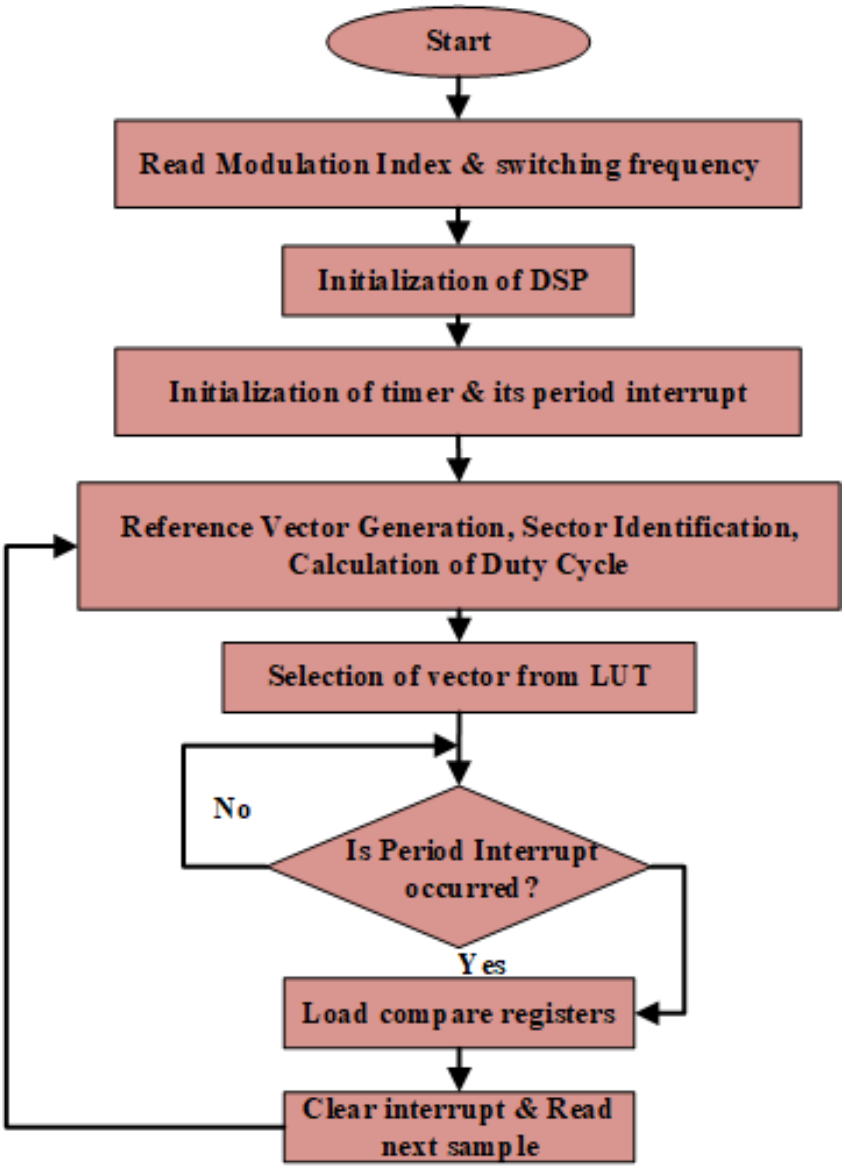
Start
Read Modulation Index & switching frequency
Initialization of DSP
Initialization of timer & its period interrupt
Reference Vector Generation, Sector Identification, Calculation of Duty Cycle
Selection of vector from LUT
No
Is Period Interrupt occurred ?
Yes
Load compare registers
Clear interrupt & Read next sample

Fig. 5.1 Flowchart of SVPWM Algorithm

5.2 Experimental Analysis

The theoretical results obtained so far for various modulation techniques have been confirmed by a number of experimental analyses. The total harmonic distortion (THD) as of right now is the figure of merit. A detailed explanation of the relationships between HDFs, the effect of leaky inductance on the two planes, the assessment of total THD, and the current ripple of the $\alpha - \beta$ and $x_3 - y_3$ planes may be found in [32].

A 1 HP, 4-pole, 5-phase squirrel cage induction motor serves as the foundation for the test apparatus The machine's specifications were ascertained using standard testing (no load and blocked rotor tests) at 50 Hz with the inverter supply. Table 5.1 presents the findings.

TABLE 5.1 NOMINAL PARAMETERS OF FPIM

Parameter	**Value**	**Parameter**	**Value**
Stator resistance (r_s)	1.015 Ω	Rotor resistance (r_r')	1.425 Ω
Stator leakage inductance (L_{ls})	6.1 (mH)	Rotor leakage inductance (L_{ls}')	6.1 (mH)
Mutual inductance (M)	85.73 (mH)	Number of Poles (P)	4
Moment of inertia (J)	0.158 (kg-m^2)	Nominal speed	1400 rpm

Fig. 5.2 illustrates the complete experimental setup used to evaluate the performance of the PWM control algorithms. A five-phase inverter power module (PEC16DSMO13) was employed to drive the induction machine.

The DC-link voltage was regulated and maintained at 200 V throughout the experiments. The control platform is built around the Texas Instruments Delfino TMS320F28379D LaunchPad, a high-performance digital signal processor (DSP) specifically designed for real-time motor control and power electronics applications. The induction machine was operated in an open-loop V/f (voltage-to-frequency) control mode, which maintains a constant voltage-to-frequency ratio to ensure a linear torque-speed relationship under no-load conditions.

To comprehensively assess the system's performance under varying modulation and frequency conditions, the modulation index and the fundamental frequency are changed from M = 0.1 at f = *5* Hz to M = 1.0515 at f = *52.5* Hz. For each modulation index/frequency pair, the steady-state stator voltage and current waveforms.

These were recorded under steady-state, no-load conditions for each of the employed PWM methodologies. Furthermore, the total harmonic distortion (THD) of the phase current was computed for each operating point. The THD values were primarily measured using a YOKOGAWA WT1800 Precision Power Analyzer, known for its high-accuracy power measurements. These results were further validated through spectral analysis using the Fast Fourier Transform (FFT) technique, ensuring consistency and correctness of the harmonic evaluation.

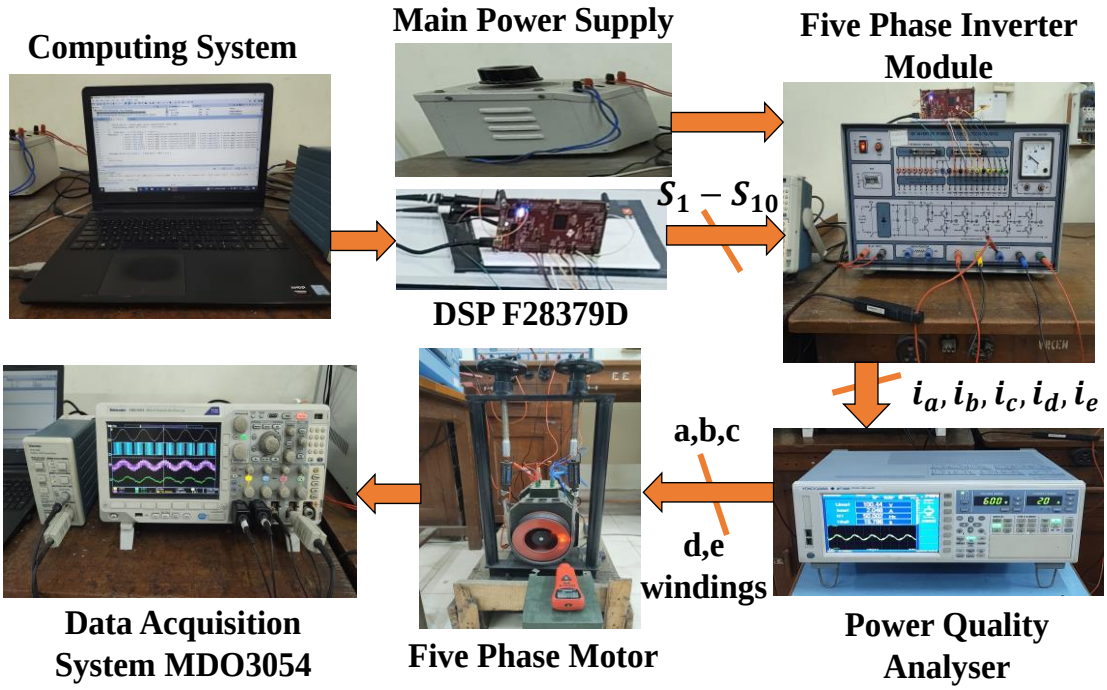

Fig.5.2 The five-phase induction motor and the power and control module are part of the experimental setup.

Fig.5.3 to Fig. 5.8 shows the phase "a" current waveform for CSVPWM, Clamp 36°, Clamp 18°, Clamp 36°_APCPWM_03, Clamp 18°_APCPWM_03 concerning their THD spectrum. The harmonic components of CSVPWM revolve around frequencies that are equal to or greater than the switching frequency. However, the spectra are more dispersed when using the suggested APCPWM techniques. The inverter dead time effect causes lower order harmonics [32], which are visible in the harmonic spectrum because the inverter is run in real-time open-loop V/f mode. Figures 5.3 through 5.8 display the experimental findings of the measured rms current ripple across the linear modulation range at a constant V/f ratio.

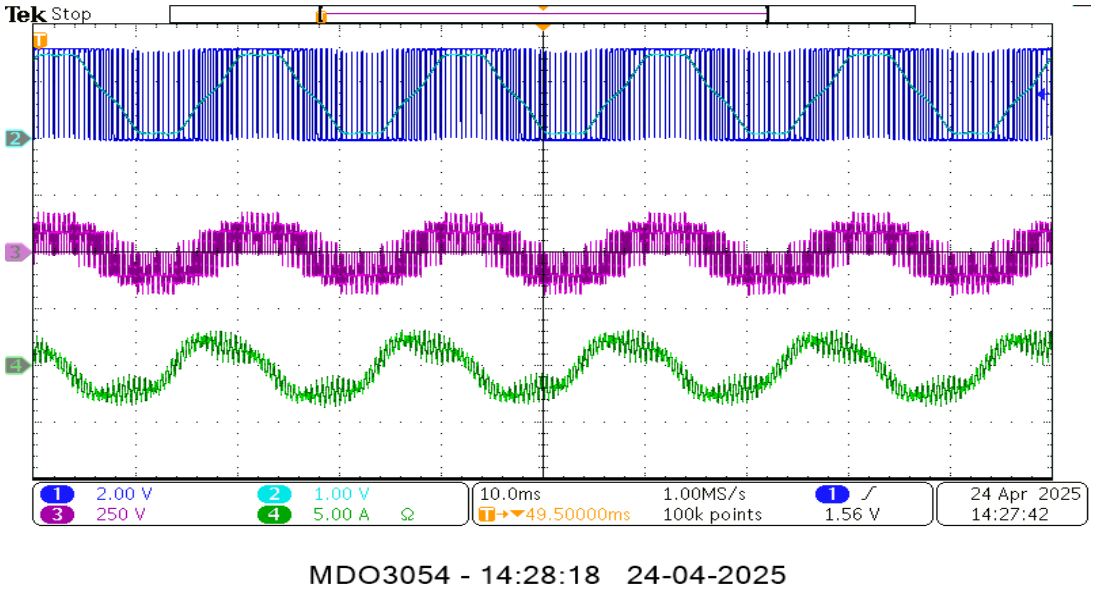

(a)

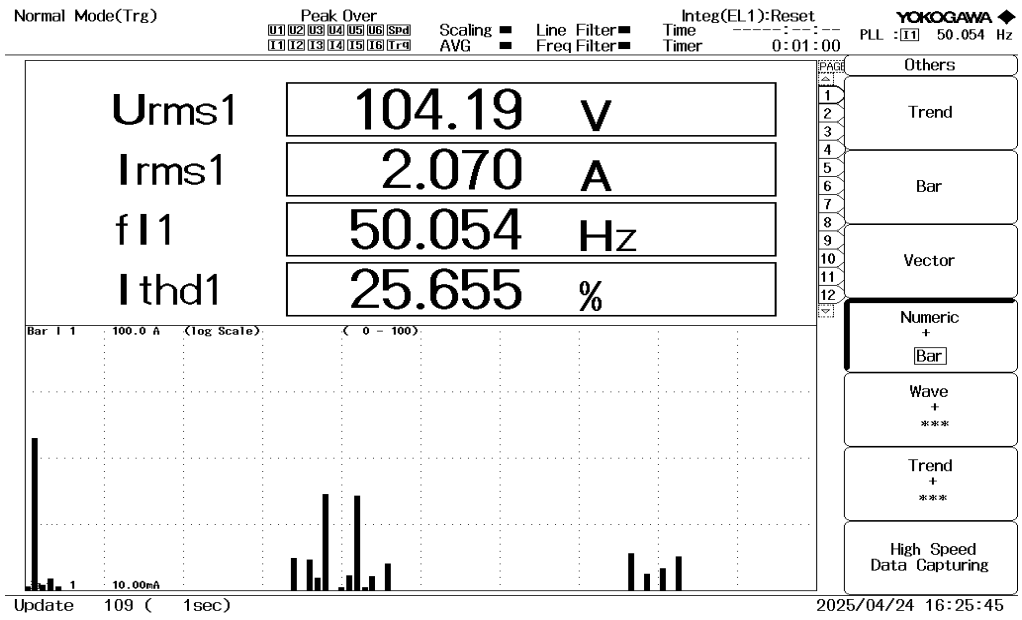

(b)

Fig. 5.3 (a) Waveforms for CSVPWM (Top to bottom, Gate Pulse (10.0ms/div, 2.0v/div), Phase Voltage (10.0ms/div, 250.0v/div), Phase Current (10.0ms/div, 5.0A/div) (b) respective Phase current THD spectrum

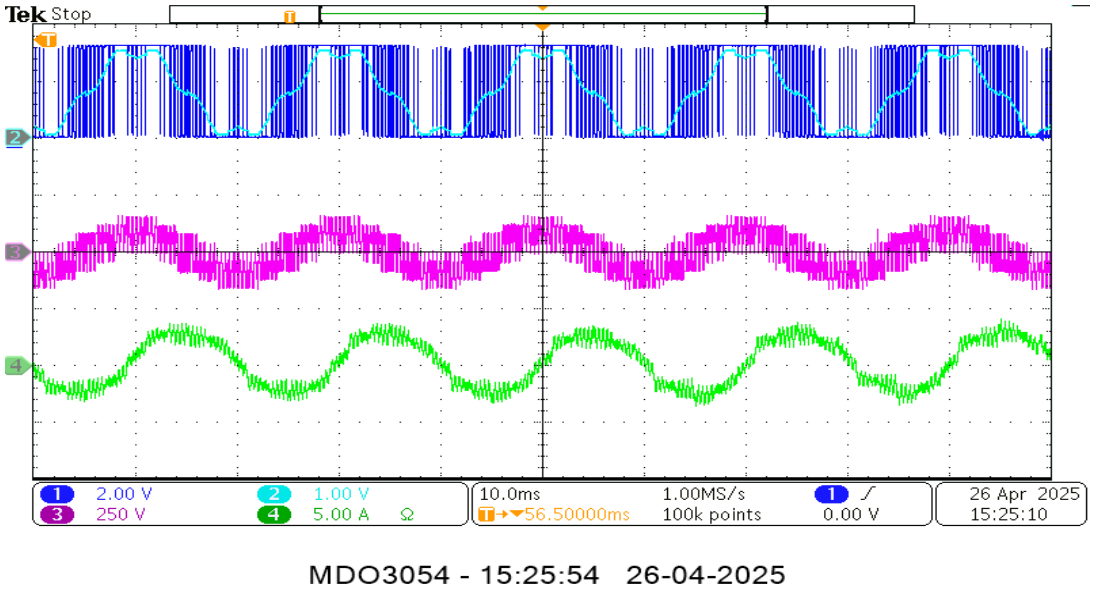

(a)

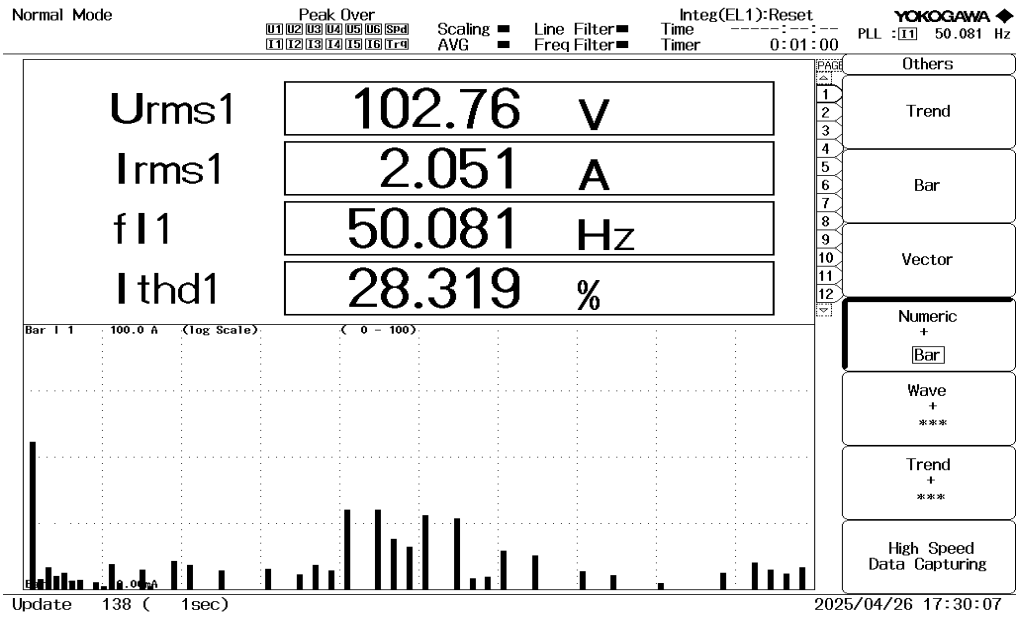

(b)

Fig. 5.4 (a) Waveforms for Clamp 18° (Top to bottom, Gate Pulse (10.0ms/div, 2.0v/div), Phase Voltage (10.0ms/div, 250.0v/div), Phase Current (10.0ms/div, 5.0A/div) (b) respective Phase current THD spectrum

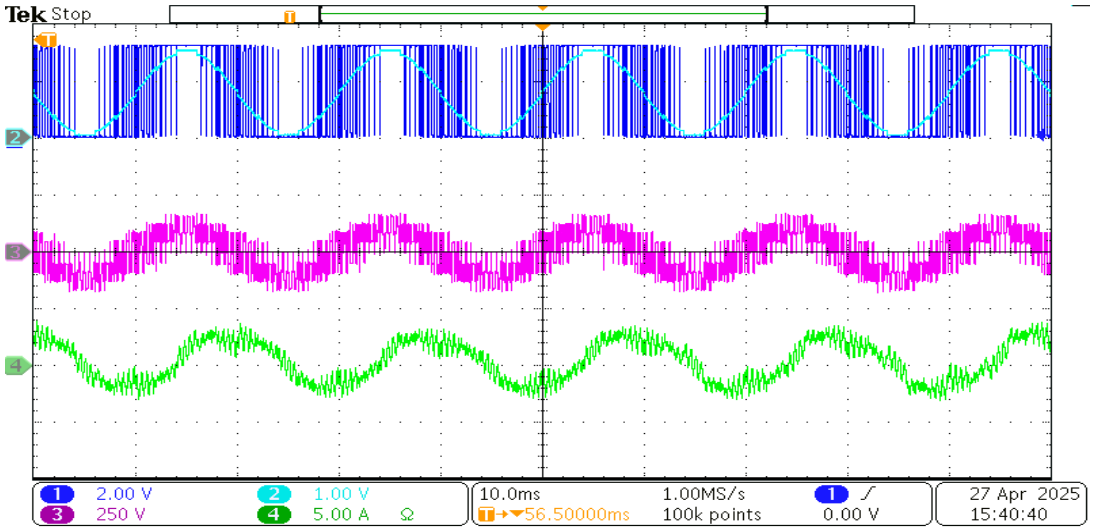

(a)

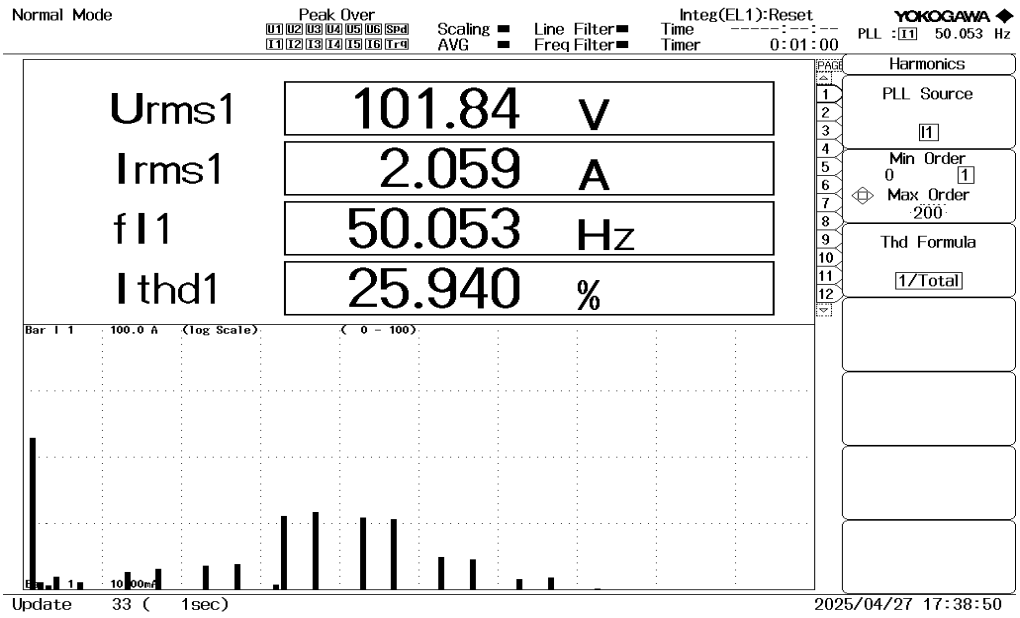

(b)

Fig. 5.5 (a) Waveforms for Clamp 36° (Top to bottom, Gate Pulse (10.0ms/div, 2.0v/div), Phase Voltage (10.0ms/div, 250.0v/div), Phase Current (10.0ms/div, 5.0A/div) (b) respective Phase current THD spectrum

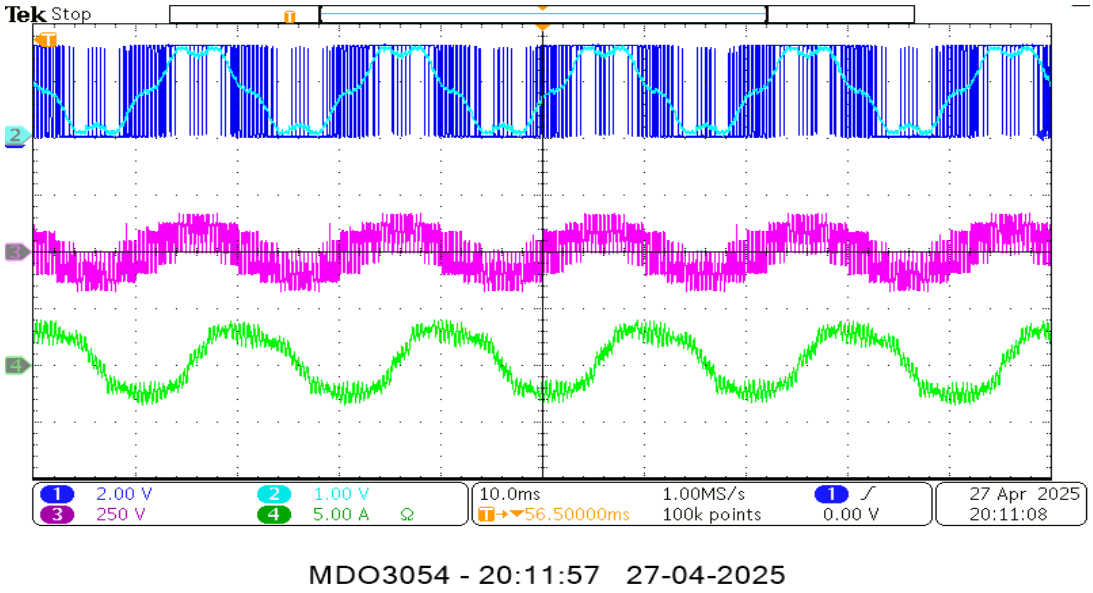

(a)

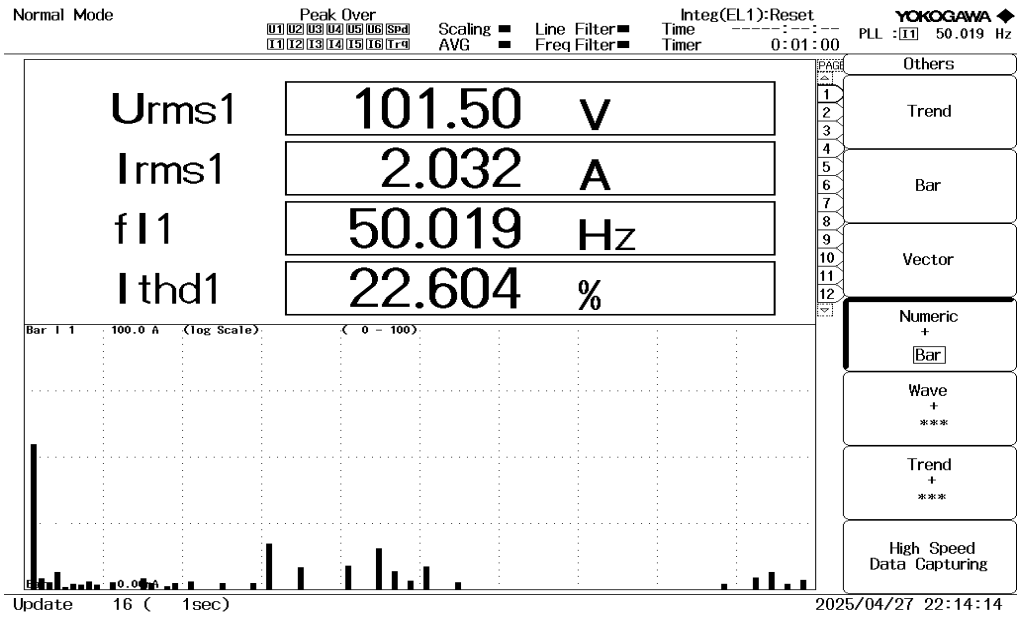

(b)

Fig. 5.6 (a) Waveforms for Clamp 18°_APCPWM_03 (Top to bottom, Gate Pulse (10.0ms/div, 2.0v/div), Phase Voltage (10.0ms/div, 250.0v/div), Phase Current (10.0ms/div, 5.0A/div) (b) respective Phase current THD spectrum

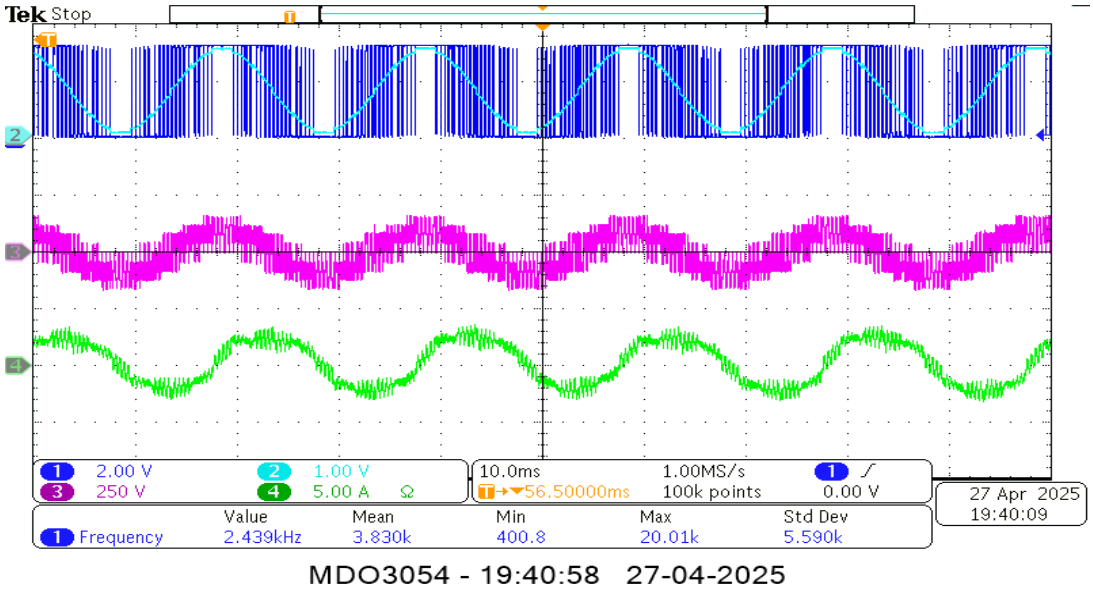

(a)

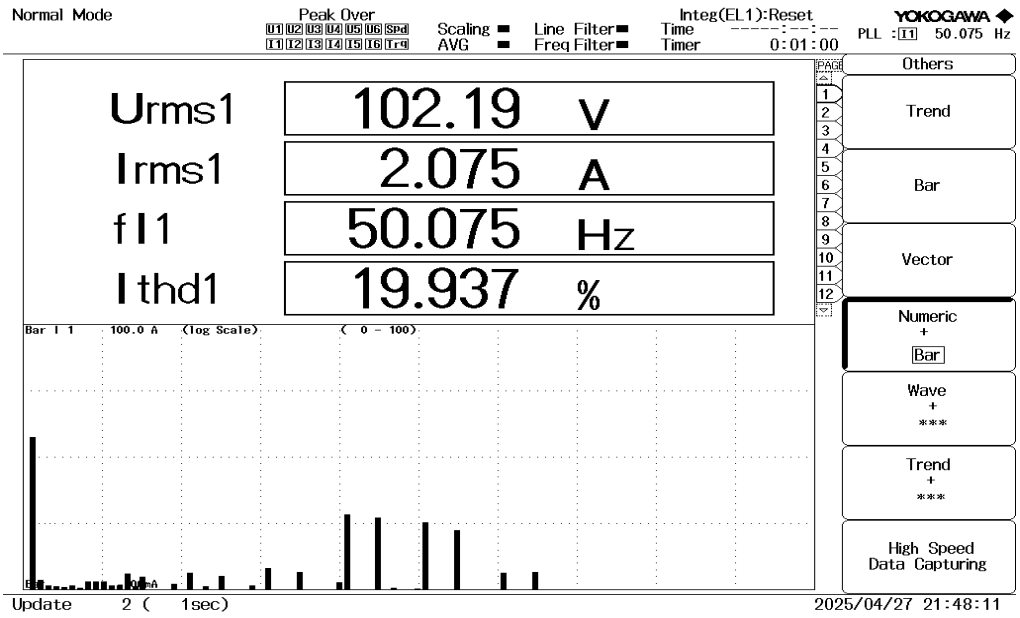

(b)

Fig. 5.7 (a) Waveforms for Clamp 36°_APCPWM_03 (Top to bottom, Gate Pulse (10.0ms/div, 2.0v/div), Phase Voltage (10.0ms/div, 250.0v/div), Phase Current (10.0ms/div, 5.0A/div) (b) respective Phase current THD spectrum

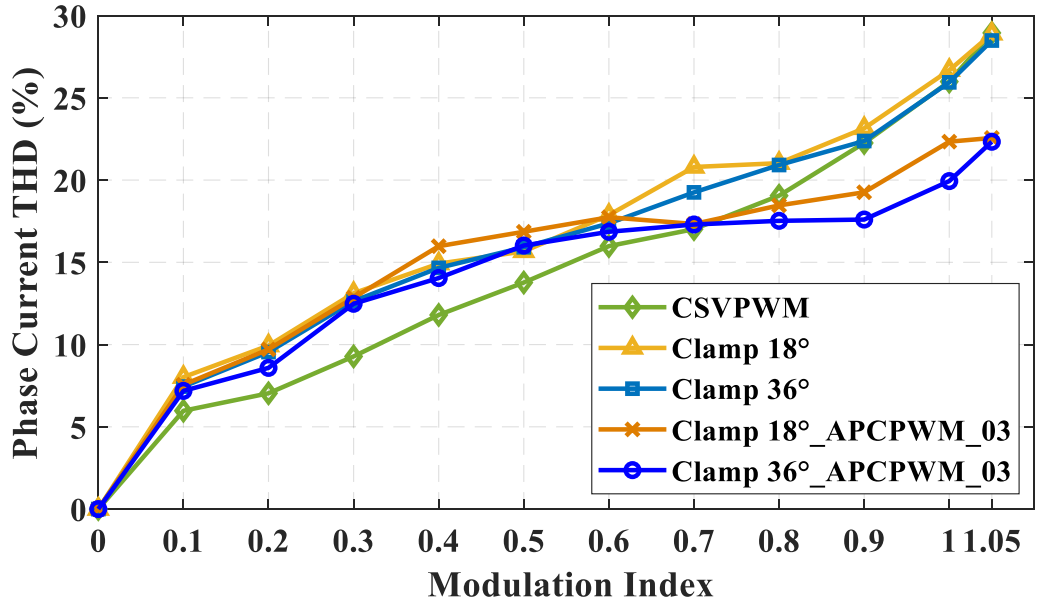

Fig.5.8 Experimental results. Stator current THD versus modulation index for 36°_*APCPWM*_03 with the conventional CSVPWM, BCPWMs, APCPWM_01 and APCPWM_02

The graphical representation illustrates the variation of total harmonic distortion (THD) in phase current for different PWM techniques within the linear modulation range, specifically for modulation indices ranging from m=0.1m = 0.1m=0.1 to m=1m = 1m=1. As observed from the plot, each PWM technique exhibits a distinct THD profile as a function of mmm.

Generally, THD decreases with increasing mmm, reaching its minimum near the upper boundary of the linear modulation region, where inverter voltage utilization is maximized. Among the compared techniques, [insert PWM technique name] demonstrates superior harmonic performance, exhibiting the lowest THD throughout the range. The THD values were experimentally measured using a YOKOGAWA WT1800 Precision Power Analyzer and validated using FFT analysis, showing strong agreement with theoretical predictions and simulation results.

This correlation between theoretical and experimental findings confirms the accuracy of the proposed modulation methodologies and validates the fidelity of the real-time implementation on the TMS320F28379D DSP platform. The results reinforce the effectiveness of these PWM techniques in achieving high-quality output with minimal harmonic distortion under linear modulation conditions.

Along with that, Table 5.2 provides a relative comparison of Clamp 36° APCPWM_03 method with CSVPWM at a higher modulation index, showing a significant reduction in phase current harmonics.

TABLE 5.2

Phase current THD performance evaluation of PWM systems under high modulation index operation

Modulation Index(m)	CSVPWM	Clamp 18° APCPWM_03	(%) THD Reduction	Clamp 36° APCPWM_03	(%) THD Reduction
0.8	19.052	18.46	3.107	17.523	8.025
0.9	22.255	19.259	13.462	17.6	20.9166
1.0	25.985	22.334	14.050	19.937	23.274
1.05	29.945	22.56	24.66	21.33	28.769

From the preceding analysis, it is evident that the selection of an appropriate switching sequence within a PWM sub-cycle plays a crucial role in minimizing current ripple. This decision is not solely dependent on the magnitude of the reference vector but also on its angular position within the switching cycle.

Since the effectiveness of a given PWM strategy varies with the reference vector's location in the modulation plane, a fixed sequence approach may not yield optimal results across all operating conditions.

Therefore, it becomes essential to implement a dynamic selection mechanism that can adaptively choose the most suitable sequence for a given vector. To achieve this, a two-zone hybrid PWM technique is proposed. This method divides the modulation region into two distinct zones based on the modulation index and the angular sector of the reference vector

CHAPTER 5
CONCLUSION

This study focuses on the development and application of advanced phase clamping switching sequences combined with space vector-based PWM generation to reduce current ripple in five-phase induction motor drives. Traditional PWM methods, while effective to some extent, often struggle to maintain low harmonic distortion under varying operating conditions, especially at high modulation indices. To address this challenge, the research proposes a novel hybrid PWM technique that integrates conventional switching sequences with advanced bus clamping PWM (APCPWM) strategies. By blending these methods, the hybrid approach aims to leverage the strengths of both to achieve a significant reduction in current harmonic content and improve the overall performance of multiphase drives.

The analytical framework presented in this study builds on prior research involving continuous and discontinuous PWM methods, extending these concepts to incorporate advanced bus clamping sequences within a five-phase motor drive environment. The investigation correlates the advanced PWM strategies with conventional ones, contextualizing the analysis within a three-phase system driven by a two-level voltage source inverter (VSI) to draw parallels and validate the approach. A comprehensive evaluation of current ripple is conducted across different PWM schemes, including conventional space vector PWM (CSVPWM), bus clamping PWM (BCPWM), and various advanced phase clamping PWM (APCPWM) sequences. These evaluations utilize the (2L+2M) vector selection technique, which allows for precise switching state determination and optimization of harmonic performance.

Both theoretical analysis and experimental results strongly support the effectiveness of the proposed two-zone hybrid PWM technique. Experimental validation on a V/f controlled induction motor drive operating at rated voltage and frequency consistently demonstrates approximately a 23% reduction in phase current total harmonic distortion (THD) compared to conventional CSVPWM. This improvement highlights the robustness of the hybrid approach in mitigating current ripple and enhancing power quality. Consequently,

the study underscores the practical applicability of the proposed PWM method for advanced multiphase motor drive systems, promising improved efficiency, reduced thermal stress, and smoother motor operation under a wide range of operating conditions.

Bibliography

[1] Holtz, J., “Pulsewidth modulation for electronic power conversion”, *Proceedings of the IEEE,* vol.82, no.8, pp.1194-1214, August 1994.

[2] Trzynadlowski, A.M., "An overview of modern PWM techniques for three-phase, voltage-controlled, voltage-source inverters," *Industrial Electronics, 1996. ISIE '96., Proceedings of the IEEE International Symposium on* , vol.1, no., pp.25-39 , Jun 1996

[3] Keliang Zhou and Danwei Wang, "Relationship between space-vector modulation and three-phase carrier-based PWM: a comprehensive analysis [three-phase inverters]," *Industrial Electronics, IEEE Transactions on* , vol.49, no.1, pp.186-196, Feb 2002

[4] Narayanan, G and Ranganathan, “Triangle-Comparison Approach and Space Vector Approach to Pulsewidth Modulation in Inverter fed Drives,*” Journal of the Indian Institute of Science,* 80, pp. 409-427, 2000.

[5] Ward, E.E.; Harer, H., "Preliminary investigation of an invertor-fed 5-phase induction motor," *Electrical Engineers, Proceedings of the Institution of* , vol.116, no.6, pp.980-984, June 1969

[6] Singh, G.K., “Multi-phase induction machine drive research- a survey,” *Electr. Power Syst. Res.,* vol.61, pp.139-147, 2002.

[7] Levi, E., Bojoi, R., Profumo, F., Toliyat, H.A. and Williamson, S., "Multiphase induction motor drives - a technology status review," *Electric Power Applications, IET* , vol.1, no.4, pp.489,516, July 2007.

[8] Fudeh, H. R. and Ong, C.M., "Modeling and Analysis of Induction Machines Containing Space Harmonics Part I: Modeling and Transformation," *Power Apparatus and Systems, IEEE Transactions on* , vol.102, no.8, pp.2608-2615, Aug. 1983

[9] De Silva, P.S.N., Fletcher, J.E. and Williams, B.W., "Development of space vector modulation strategies for five phase voltage source inverters," *Power Electronics,*

Machines and Drives, 2004. (PEMD 2004). Second International Conference on (Conf. Publ. No. 498) , vol.2, no., pp.650-655, 2004.

[10] Kelly, J.W., Strangas, E.G. and Miller, J.M., "Multiphase space vector pulse width modulation," *Energy Conversion, IEEE Transactions on* , vol.18, no.2, pp.259-264, June 2003

[11] Hyung-Min Ryu, Jang-Hwan Kim and Seung-Ki Sul, "Analysis of multiphase space vector pulse width modulation based on multiple d-q spaces concept," *Power Electronics and Motion Control Conference, 2004. IPEMC 2004. The 4th International* , vol.3, no., pp.1618-1624 Vol.3, Aug. 2004.

[12] Iqbal, A., Levi, E., Jones, M. and Vukosavic, S.N., "Generalised Sinusoidal PWM with Harmonic Injection for Multi-Phase VSIs," *Power Electronics Specialists Conference, 2006. PESC '06. 37th IEEE* , vol., no., pp.1,7, 18-22 June 2006

[13] G. Narayanan and V. T. Ranganathan, “Two novel synchronized bus-clamping PWM strategies based on space vector approach for high power drives,” in IEEE Transactions on Power Electronics, vol. 17, no. 1, pp. 84-93, Jan. 2002, doi:10.1109/63.988673.

[14] G. Narayanan, H. K. Krishnamurthy, D. Zhao and R. Ayyanar, “Advanced bus-clamping PWM techniques based on space vector approach,” in IEEE Transactions on Power Electronics, vol. 21, no. 4, pp. 974-984, July 2006, doi:10.1109/TPEL.2006.876854.

[15] T. Bhavsar and G. Narayanan, “Harmonic Analysis of Advanced Bus-Clamping PWM Techniques,” in IEEE Transactions on Power Electronics, vol. 24, no. 10, pp. 2347-2352, Oct. 2009, doi: 10.1109/TPEL.2009.2013492.

[16] S. A. Sadale and R. Karampuri, "Performance Analysis of Five-Phase System for Various Bus-Clamping Space Vector Based Pulse Width Modulation Methods," 2024 Third International Conference on Power, Control and Computing Technologies (ICPC2T), Raipur, India, 2024, pp. 157-162, doi: 10.1109/ICPC2T60072.2024.10474966

[17] D. G. Holmes and T. A. Lipo, “IEEE press series on power engineering”, in Pulse Width Modulation for Power Converters: Principles and Practice. Hoboken, NJ, USA: Wiley-IEEE Press, 2003.

[18] A. M. Hava, R. J. Kerkman and T. A. Lipo, "A high-performance generalized discontinuous PWM algorithm," in IEEE Transactions on Industry Applications, vol. 34, no. 5, pp. 1059-1071, Sept.-Oct. 1998, doi: 10.1109/28.720446.

[19] L. Asiminoaei, P. Rodriguez and F. Blaabjerg, "Application of Discontinuous PWMModulation in Active Power Filters," in IEEE Transactions on Power Electronics, vol. 23, no. 4, pp. 1692-1706, July 2008, doi: 10.1109/TPEL.2008.924599.

[20] Toliyat, H.A., Lipo, T.A. and White, J.C., "Analysis of a concentrated winding induction machine for adjustable speed drive applications. I. Motor analysis," *Energy Conversion, IEEE Transactions on* , vol.6, no.4, pp.679-683, 1991

[21] Iqbal, A. and Moinuddin, S., "Comprehensive Relationship Between Carrier-Based PWM and Space Vector PWM in a Five-Phase VSI," *Power Electronics, IEEE Transactions on* , vol.24, no.10, pp.2379-2390, Oct. 2009

[22] Iqbal, A. and Khan, M.A., "A simple approach to space vector pwm signal generation for a five-phase voltage source inverter," *India Conference, 2008. INDICON 2008. Annual IEEE* , vol.2, no., pp.418-424, 2008

[23] Hongwei Gao, Jianyong Su, Guijie Yang and Jian Liu, "SVPWM equivalent algorithm based on carrier for five-phase voltage source inverter," *Power Electronics and Motion Control Conference (IPEMC), 2012 7th International* , vol.1, no., pp.758-762, 2012

[24] *23.* K. Basu, J. S. S. Prasad and G. Narayanan, “Minimization of Torque Ripple in PWM AC Drives,” in IEEE Transactions on Industrial Electronics, vol. 56, no. 2, pp. 553-558, Feb. 2009, doi: 10.1109/TIE.2008.2004391.

[25] S. A. Sadale, D. R. Dhore and R. Karampuri, "Improved Phase-Clamping PWM Techniques with Space Vector Approach for Five-Phase System," 2024 IEEE International Conference on Power Electronics, Drives and Energy Systems (PEDES), Mangalore, India, 2024, pp. 1-6, doi: 10.1109/PEDES61459.2024.10961144.

[26] G. Narayanan, H. K. Krishnamurthy, D. Zhao and R. Ayyanar, “Advanced bus-clamping PWM techniques based on space vector approach,” in IEEE Transactions on Power Electronics, vol. 21, no. 4, pp. 974-984, July 2006, doi:10.1109/TPEL.2006.876854.

[27] T. Bhavsar and G. Narayanan, “Harmonic Analysis of Advanced Bus-Clamping PWM Techniques,” in IEEE Transactions on Power Electronics, vol. 24, no. 10, pp. 2347-2352, Oct. 2009, doi: 10.1109/TPEL.2009.2013492.

[28] G. Narayanan and V. T. Ranganathan, “Analytical evaluation of harmonic distortion in PWM AC drives using the notion of stator flux ripple,” in IEEE Transactions on Power Electronics, vol. 20, no. 2, pp. 466-474, March 2005, doi:10.1109/TPEL.2004.842961.

[29] K. Basu, J. S. S. Prasad, G. Narayanan, H. K. Krishnamurthy and R. Ayyanar, “Reduction of Torque Ripple in Induction Motor Drives Using an Advanced Hybrid PWM Technique,” in IEEE Transactions on Industrial Electronics, vol. 57, no. 6, pp. 2085-2091, June 2010, doi: 10.1109/TIE.2009.2034183.

[30] D. Zhao, V. S. S. P. K. Hari, G. Narayanan and R. Ayyanar, “Space-Vector-Based Hybrid Pulsewidth Modulation Techniques for Reduced Harmonic Distortion and Switching Loss,” in IEEE Transactions on Power Electronics, vol. 25, no. 3, pp. 760-774, March 2010, doi: 10.1109/TPEL.2009.2030200.

[31] D. Dujic, M. Jones and E. Levi, "Analysis of Output Current Ripple rms in Multiphase Drives Using Space Vector Approach," in IEEE Transactions on Power Electronics, vol. 24, no. 8, pp. 1926-1938, Aug. 2009, doi: 10.1109/TPEL.2009.2017746.

[32] D. Dujic, M. Jones, E. Levi, J. Prieto and F. Barrero, "Switching Ripple Characteristics of Space Vector PWM Schemes for Five-Phase Two-Level Voltage Source Inverters—Part 1: Flux Harmonic Distortion Factors," in IEEE Transactions on Industrial Electronics, vol. 58, no. 7, pp. 2789-2798, July 2011, doi: 10.1109/TIE.2010.2070777.

[33] M. Jones, D. Dujic, E. Levi, J. Prieto and F. Barrero, "Switching Ripple Characteristics of Space Vector PWM Schemes for Five-Phase Two-Level Voltage Source Inverters—Part 2: Current Ripple," in IEEE Transactions on Industrial Electronics, vol. 58, no. 7, pp. 2799-2808, July 2011, doi: 10.1109/TIE.2010.2070778.

[34] J. Prieto, M. Jones, F. Barrero, E. Levi and S. Toral, "Comparative Analysis of Discontinuous and Continuous PWM Techniques in VSI-Fed Five-Phase Induction Motor," in IEEE Transactions on Industrial Electronics, vol. 58, no. 12, pp. 5324-5335, Dec. 2011, doi: 10.1109/TIE.2011.2126540.

[35] R. Karampuri, S. Jain and V. T. Somasekhar, "Common-Mode Current Elimination PWM Strategy Along With Current Ripple Reduction for Open-Winding Five-Phase Induction Motor Drive," in *IEEE Transactions on Power Electronics*, vol. 34, no. 7, pp. 6659-6668, July 2019, doi: 10.1109/TPEL.2018.2873692.